# Synergetic use of IASI and TROPOMI space borne sensors for generating a tropospheric methane profile product

Matthias Schneider[1], Benjamin Ertl[1,2], Christopher J. Diekmann[1], Farahnaz Khosrawi[1], Amelie N. Röhling[1], Frank Hase[1], Darko Dubravica[1], Omaira E. García[3], Eliezer Sepúlveda[3], Tobias Borsdorff[4], Jochen Landgraf[4], Alba Lorente[4], Huilin Chen[5], Rigel Kivi[6], Thomas Laemmel[7,*], Michel Ramonet[7], Martin Steinbacher[8], Frank Meinhardt[9], Nicholas M. Deutscher[10], David W. T. Griffith[10], Voltaire A. Velazco[10,**], and David F. Pollard[11]

[1]Institute of Meteorology and Climate Research (IMK-ASF), Karlsruhe Institute of Technology, Karlsruhe, Germany
[2]Steinbuch Centre for Computing (SCC), Karlsruhe Institute of Technology, Karlsruhe, Germany
[3]Izaña Atmospheric Research Center, Agencia Estatal de Meteorología (AEMET), Santa Cruz de Tenerife, Spain
[4]Earth Science Group, SRON Netherlands Institute for Space Research, Utrecht, The Netherlands
[5]Center for Isotope Research, University of Groningen, Groningen, The Netherlands
[6]Space and Earth Observation Centre, Finnish Meteorological Institute, Sodankylä, Finland
[7]Laboratoire des Sciences du Climat et de l'Environnement (LSCE), CEA, 91191 Gif sur Yvette, France
[8]Swiss Federal Laboratories for Materials Science and Technology (EMPA), Dübendorf, Switzerland
[9]Air Monitoring Network, Federal Environment Agency (UBA), Langen, Germany
[10]Centre for Atmospheric Chemistry, School of Earth, Atmospheric and Life Sciences, Faculty of Science, Medicine and Health, University of Wollongong, Wollongong, Australia
[11]National Institute of Water and Atmospheric Research Ltd (NIWA), Lauder, New Zealand
[*]now at: Laboratory for the Analysis of Radiocarbon with AMS (LARA) Department of Chemistry, Biochemistry and Pharmaceutical Sciences (DCBP) & Oeschger Centre for Climate Change Research (OCCR), University of Bern, Switzerland
[**]now at: Deutscher Wetterdienst (DWD), Albin-Schwaiger-Weg 10, Hohenpeissenberg, Germany

**Correspondence:** M. Schneider
(matthias.schneider@kit.edu)

**Abstract.** The thermal infrared nadir spectra of IASI (Infrared Atmospheric Sounding Interferometer) are successfully used for retrievals of different atmospheric trace gas profiles. However, these retrievals offer generally reduced information about the lowermost tropospheric layer due to the lack of thermal contrast close to the surface. Spectra of scattered solar radiation observed in the near and/or short wave infrared, for instance by TROPOMI (TROPOspheric Monitoring Instrument) offer higher sensitivity near ground and are used for the retrieval of total column averaged mixing ratios of a variety of atmospheric trace gases. Here we present a method for the synergetic use of IASI profile and TROPOMI total column data. Our method uses the output of the individual retrievals and consists of linear algebra a posteriori calculations (i.e. calculation after the individual retrievals). We show that this approach is largely equivalent to applying the spectra of the different sensors together in a single retrieval procedure, but with the substantial advantage of being applicable to data generated with different individual retrieval processors, of being very time efficient, and of directly benefiting from the high quality and most recent improvements of the individual retrieval processors.

We demonstrate the method exemplarily for atmospheric methane ($CH_4$). We perform a theoretical evaluation and show that the a posteriori combination method yields a total column averaged $CH_4$ product ($XCH_4$) that conserves the good sensitivity of

the corresponding TROPOMI product while merging it with the upper tropospheric and lower stratospheric (UTLS) $CH_4$ partial column information of the corresponding IASI product. As consequence, the combined product offers in addition sensitivity for the tropospheric $CH_4$ partial column, which is not provided by the individual TROPOMI nor the individual IASI product. The theoretically predicted synergetic effects are verified by comparisons to $CH_4$ reference data obtained from collocated $XCH_4$ measurements at five globally distributed TCCON (Total Carbon Column Observing Network) stations, $CH_4$ profile measurements made by 24 individual AirCore soundings, and lower tropospheric $CH_4$ data derived from continuous ground-based in-situ observations made at two nearby Global Atmospheric Watch (GAW) mountain stations. The comparisons clearly demonstrate that the combined product can reliably detect $XCH_4$ signals and allows to distinguish between tropospheric and UTLS $CH_4$ partial column averaged mixing ratios, which is not possible by the individual TROPOMI and IASI products. We find indications of a weak positive bias of $+1.7\pm1.2\%$ of the combined lower tropospheric data product with respect to the references. For the UTLS $CH_4$ partial columns we find no significant bias and a scatter with respect to the reference data sets of below $1\%$.

## 1 Introduction

Measurements from different ground- or satellite-based sensors target at the observations of the same atmospheric parameters (e.g. the same trace gases), but with different characteristics (e.g. sensitivities for different vertical regions). Often the different sensors use different observation geometries (limb scanning, nadir, solar light reflected at the Earth's surface) and/or different spectral regions (e.g. UV/vis, near infrared, thermal infrared, microwave). Dedicated experts and efforts are needed to develop retrieval techniques that are specifically optimized for an individual sensor. An algorithm that uses coincident measurements of all the different sensors for a multispectral approach for the optimal estimation of the atmospheric state would well exploit the synergies of the different observation geometries and spectral regions and thus allows for detecting the atmospheric state in more detail than achievable by individual optimal estimation retrievals.

Cuesta et al. (2013) present such 'super retrieval', which performs an optimal estimation of atmospheric ozone ($O_3$) applying the spectra measured by the thermal nadir sensor IASI (Infrared Atmospheric Sounding Interferometer) and the UV/vis sensor GOME (Global Ozone Monitoring Experiment). Their publication shows that using the multispectral approach allows the detection of lower tropospheric $O_3$, which is not possible by an individual usage of the IASI and GOME spectra. Costantino et al. (2017) showed that the quality of this multispectral lower tropospheric $O_3$ product can be further improved with improved thermal nadir and UV/vis sensors.

2-1 The development of these 'super retrievals' requires experts in different remote sensing techniques to work closely together. Furthermore, as soon as measurements from a new sensor become available (or as soon as sensors are modified/improved) such super retrieval processors have to be adapted accordingly, i.e. continuous collaborative retrieval developments are required. While this is certainly possible, it might be not the most efficient way. The optimal exploitation of the already available individual retrieval results would be much less computationally expensive than running dedicated combined retrievals.

3-1

Efficient a posteriori combination methods of individual retrieval products are currently of high interest, because the steadily increasing amount of available satellite data offers more and more possibilities for synergetic use. Worden et al. (2015) combines the thermal and near infrared observations of methane ($CH_4$) made by TES (Thermal Emission Spectrometer) and GOSAT (Greenhouse gas mOnitoring SATellite), respectively, by performing approximative calculations and with a focus on monthly mean data. Data aggregation is necessary due to the reduced temporal and horizonal coverage of TES and GOSAT and their imperfect collocation. The method of Ceccherini et al. (2009) focuses on avoiding uncertainties in the combined product due to constraints and vertical interpolation, which might be a problem when combining two vertically resolved profile products generated applying different constraints. However, this method needs the Jacobians (changes in the spectra caused by changes in the atmospheric state) of the retrieved products, which are large matrices that are generally not stored in operational retrieval output files. Cortesi et al. (2016) applied this approach for combining the thermal infrared MIPAS-STR (Michelson Interferometer for Passive Atmospheric Sounding - STRatospheric aircraft) and microwave MARSCHALS (Millimetre-wave Airborne Receivers for Spectroscopic Characterisation in Atmospheric Limb Sounding) aircraft-based remote sensing products of $O_3$, nitric acid ($HNO_3$), water vapour ($H_2O$), and atmospheric temperature.

Here, we propose to generate a multi-sensor optimal estimation $CH_4$ profile product by simple a posteriori calculations using available outputs of IASI and TROPOMI (Tropospheric Monitoring Instrument) retrievals. The method allows a computationally very efficient generation of global daily maps of the combined data product and only needs the individually retrieved states, averaging kernels and noise covariances provided by the respective remote sensing experts in the context of their standard retrieval work. The proposed method can be used flexibly for combining measurement information of different satellite sensors. For most cases the method approximates closely a dedicated combined optimal estimation retrieval that uses the combined IASI and TROPOMI spectra as input.

The reliable and global detection of tropospheric $CH_4$ independently from $CH_4$ at higher altitudes can lead to an improved understanding of the $CH_4$ cycle. Respective data allow a more direct investigation of the $CH_4$ boundary layer source and sink signals than total column averaged mixing ratios ($XCH_4$) provided globally for instance by GOSAT (e.g. Parker et al., 2020) or TROPOMI (Lorente et al., 2020). This is because $XCH_4$ signals are strongly affected by vertical shifts of the tropopause altitude, i.e. their use for investigating $CH_4$ absorption and release at ground depends on the correct consideration of the tropopause altitude by model simulations (Pandey et al., 2016).

3-2

This manuscript is organised as follows. Section 2 briefly discusses the used IASI and TROPOMI products (generated by two individual retrievals), presents the equations for the optimal a posteriori combination of the two independent retrieval outputs, and performs a theoretical evaluation of the individual and combined products. Section 3 validates the total column and tropospheric and UTLS (upper tropospheric/lower stratospheric) partial column products obtained by the individual IASI and TROPOMI retrievals and by the a posteriori combination. Section 4 resumes the results of our study and briefly discusses upcoming possibilities. Furthermore, in Appendix A we provide extensive background information on the theory of our a posteriori combination method and we show that the method is equivalent to performing a full multispectral optimal estimation retrieval. Appendix B introduces the operator for transferring logarithmic scale differentials into linear scale differentials. Appendix C presents the operators used for converting vertical profile data into total and partial column data.

## 2 A posteriori combination of MUSICA IASI $CH_4$ and TROPOMI $XCH_4$ products

In this section we present the method for combining $CH_4$ profiles derived from IASI thermal nadir spectra and $XCH_4$ data obtained from the analysis of the near and short wave infrared spectra measured by TROPOMI.

The TROPOMI $XCH_4$ data used in this study are generated by the RemoTeC algorithm (Butz et al., 2011), which is used for the operational processing of Sentinel 5 Precursor/TROPOMI $XCH_4$ data (Hu et al., 2016; Hasekamp et al., 2019; Landgraf et al., 2019). The current operational processing algorithm version is 1.2.0. Here we use data from version 1.3.0 with the improvements as presented and validated in Lorente et al. (2020). It is foreseen to become the operational processing version with the operational processor update in April 2021. The TROPOMI output files provide the $XCH_4$ data together with the used a priori data (constructed from simulations of the global chemistry-transport model TM5, Krol et al., 2005), the column averaging kernels, and the error values. In order to filter out data with reduced quality, here we only use TROPOMI data, for which the variable `qa_value` has values larger than 0.5. This filter is consistent to the filtering as suggested in Table A1 of Lorente et al. (2020).

As IASI $CH_4$ data product we use the data generated by the retrieval processor MUSICA (MUlti-platform remote Sensing of Isotopologues for investigating the Cycle of Atmospheric water, a European Research Council project between 2011 and 2016). The MUSICA IASI data full retrieval product encompasses trace gas profiles of $H_2O$, the $HDO/H_2O$ ratio, $N_2O$, $CH_4$, and $HNO_3$. The data have been validated in several previous studies (Schneider et al., 2016; Borger et al., 2018; García et al., 2018), and it has been shown that the $CH_4$ product can very well detect the $CH_4$ signals originating in the upper troposphere/lower stratosphere. MUSICA IASI data using processor versions 3.2.1 and 3.3.0 are currently available for the 2014 to 2020 time period and are presented in Schneider et al. (2021). This MUSICA IASI data set is best suited for a posteriori data reusage (e.g. Diekmann et al., 2021), because in addition to the retrieved trace gas profiles it contains full information on retrieval settings (a priori states and constraints) and on averaging kernel and error covariance matrices. In ~~oder~~ to ensure highest MUSICA IASI data quality, here we require the flag variable `musica_fit_quality_flag` to be set to 3 (the spectral fit of the MUSICA IASI retrieval has a good quality and the spectral rediduals are close to the instrumental noise level). Furthermore, we only use MUSICA IASI data for which the flag variable `eumetsat_cloud_summary_flag` is set to 1, which guarantees that the IASI instrumental field of view is cloud-free.

A particularity of the MUSICA IASI processor is that the trace gas inversions are performed on a logarithmic scale. In Appendix B of Schneider et al. (2021) it is shown that the MUSICA IASI retrieval can be considered as a moderately non-linear problem, in particular if the differentials (averaging kernels and covariances) are used on the logarithmic scale. In the following equations we take special care on the correct usage of the corresponding logarithmic scale differentials. Nevertheless, all equations are also applicable for retrievals made on linear scale by replacing in the following the operator $\mathbf{L}$ by the identity operator.

### 2.1 Calculation of the combined state vector

For this study we use the $CH_4$ a priori profile as provided by the TROPOMI product as the common a priori for all products (these are simulations of the global chemistry-transport model TM5, Krol et al., 2005). For this purpose we modify the MUSICA IASI product and bring it in line with the TROPOMI a priori profile choice by applying Eq. (A16).

For updating the IASI $CH_4$ profile product using the TROPOMI $XCH_4$ observation we apply a Kalman filter and obtain the combined $CH_4$ state as :

$$\hat{\boldsymbol{x}}_{\boldsymbol{C}}^{\boldsymbol{l}} = \hat{\boldsymbol{x}}_{\boldsymbol{I}}^{\boldsymbol{l}} + \mathbf{L}^{-1}\boldsymbol{m}[\hat{x}_T - \boldsymbol{a}_{\boldsymbol{T}}^{*\,T}\hat{\boldsymbol{x}}_{\boldsymbol{I}}]. \tag{1}$$

Here the vector $\hat{\boldsymbol{x}}_{\boldsymbol{I}}$ and scalar $\hat{x}_T$ are the MUSICA IASI $CH_4$ profile and the TROPOMI $XCH_4$ column averaged products. The row vector $\boldsymbol{a}_{\boldsymbol{T}}^{*\,T}$ is the total column averaged mixing ratio kernel of the TROPOMI product interpolated to the vertical grid used by the MUSICA IASI processor (for details on the interpolation see Appendix C). The state vector $\hat{\boldsymbol{x}}_{\boldsymbol{C}}^{\boldsymbol{l}}$ represents the combined $CH_4$ profile product in logarithmic scale (i.e. the MUSICA IASI $CH_4$ data updated with the TROPOMI $XCH_4$ observation). The superscript '$^l$' used with $\hat{\boldsymbol{x}}_{\boldsymbol{C}}^{\boldsymbol{l}}$ and $\hat{\boldsymbol{x}}_{\boldsymbol{I}}^{\boldsymbol{l}}$ indicates the use of the logarithmic scale. Here and in the following we will mark scalars, vectors or matrix operators that are in logarithmic scale by the superscript '$^l$'. The matrix $\mathbf{L}$ is the operator for the transformation of differentials or small changes (as given by averaging kernels or error covariances) from the logarithmic to the linear scale (for more details see Appendix B).

The column vector $\boldsymbol{m}$ is the Kalman gain operator and it is given by:

$$\boldsymbol{m} = \mathbf{L}\mathbf{S}_{\hat{\boldsymbol{x}}_{\boldsymbol{I}}}^{\mathbf{l}}\mathbf{L}^T\boldsymbol{a}_{\boldsymbol{T}}^{*}(\boldsymbol{a}_{\boldsymbol{T}}^{*\,T}\mathbf{L}\mathbf{S}_{\hat{\boldsymbol{x}}_{\boldsymbol{I}}}^{\mathbf{l}}\mathbf{L}^T\boldsymbol{a}_{\boldsymbol{T}}^{*} + S_{\hat{\boldsymbol{x}}_{\boldsymbol{T}},n})^{-1}, \tag{2}$$

with the matrix $\mathbf{S}_{\hat{\boldsymbol{x}}_{\boldsymbol{I}}}^{\mathbf{l}}$ and the scalar $S_{\hat{\boldsymbol{x}}_{\boldsymbol{T}},n}$ being the logarithmic scale retrieval noise error covariance of the MUSICA IASI $CH_4$ product and the noise error variance of the TROPOMI $XCH_4$ product, respectively. The vector operator $\boldsymbol{a}_{\boldsymbol{T}}^{*}$ is the transpose of the TROPOMI column averaging kernel, i.e. $\boldsymbol{a}_{\boldsymbol{T}}^{*} = (\boldsymbol{a}_{\boldsymbol{T}}^{*\,T})^T$.

Except for the logarithmic scale transformation, the Eqs. (1) and (2) are analogous to Eqs. (A9) and (A10). As demonstrated in Appendix A2 this kind of Kalman filter application is equivalent to an optimal estimation retrieval that uses a combined IASI and TROPOMI measurement vector. The application of this Kalman filter is possible because the MUSICA IASI data are provided with full information on a priori states, constraints, error covariances, and averaging kernels (Schneider et al., 2021), and because the TROPOMI data are provided together with their a priori state, averaging kernel, and retrieval noise error (Lorente et al., 2020).

The Kalman Gain according to Eq. (2) describes how differences between the MUSICA IASI and TROPOMI $XCH_4$ product are used to update the MUSICA IASI $CH_4$ profile. An example for a Kalman Gain operator is depicted in Fig. 1. It shows that a positive difference of $+1$ ppb of $[\hat{x}_T - \boldsymbol{a}_{\boldsymbol{T}}^{*\,T}\hat{\boldsymbol{x}}_{\boldsymbol{I}}]$ will lead to a combined $CH_4$ profile product that has been modified with respect to the MUSICA IASI $CH_4$ product by almost $+3$ ppb in the lowermost troposphere, by about $-0.5$ ppb at 10 km, and by about $+1$ ppb above 20 km.

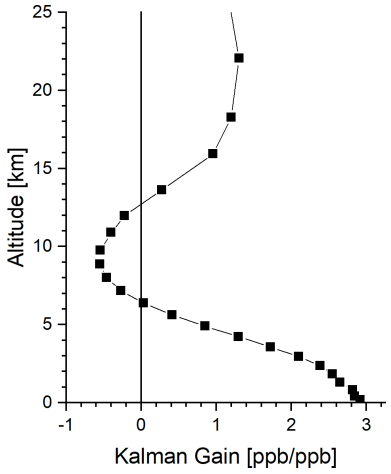


**Figure 1.** Visualisation of a Kalman Gain operator for optimally combining TROPOMI $XCH_4$ data with MUSICA IASI $CH_4$ profile data. This is the column vector $\boldsymbol{m}$ according to Eq. (2). The example shown is for a late summer atmosphere (26 September 2018) over Central Europe.

### 2.2 Collocation of TROPOMI and IASI observations

As temporal collocation criterion we use four hours, for a valid horizontal collocation the centres of the TROPOMI and IASI ground pixels must be closer than 50 km, and the difference between the ground pressure at the TROPOMI and IASI ground pixels must be within 25 hPa. Generally multiple TROPOMI/IASI ground pixel pairs fulfill the aforementioned criteria. In such case we use the pair with the smallest spatial distance, which we define as the Euclidean distance that considers a norm of 40 km for the horizontal distance and a norm of 5 hPa for the vertical distance. TROPOMI and IASI observations already belonging to a valid collocation pair are disregarded for further collocations. This ensures that an individual IASI or TROPOMI observation can only belong to a single collocation pair. The possible small difference in the TROPOMI and IASI ground pixel pressures is taken into account by using the TROPOMI ground pixel pressure during the interpolation of $\boldsymbol{a_T^*}^T$, i.e. the interpolation is made according to the TROPOMI ground pixel pressure, but according to IASI grid levels for all other altitudes.

### 2.3 Sensitivity and vertical resolution

In this section we compare the vertical representativeness of the individual retrieval products with those achieved when combining the two retrieval products. According to Eq. 1 the averaging kernels for the combined data product can be calculated as:

$$\mathbf{A_C^l} = \mathbf{A_I^l} + \mathbf{L}^{-1}\boldsymbol{m}(\boldsymbol{a_T^*}^T - \boldsymbol{a_T^*}^T\mathbf{L}\mathbf{A_I^l}\mathbf{L}^{-1})\mathbf{L}. \quad (3)$$

Here $\mathbf{A_I^l}$ and $\mathbf{A_C^l}$ are the logarithmic scale averaging kernels of the MUSICA IASI $CH_4$ product and of the combined product (the MUSICA IASI $CH_4$ product after being updated with the information provided by the TROPOMI $XCH_4$ data product),

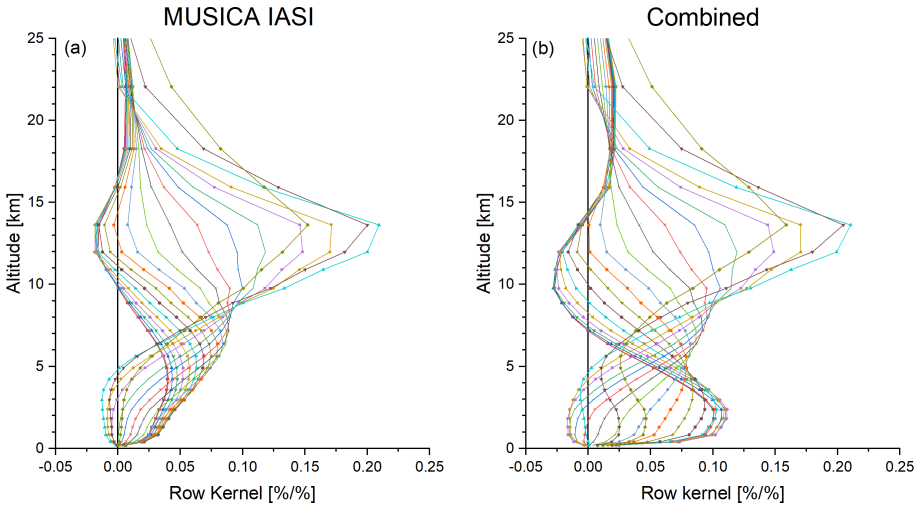


**Figure 2.** Logarithmic scale row kernels for (a) the MUSICA IASI and (b) the combined product for the same late summer observations as used in the context of Figs. 1 and 3.

respectively. These are the kernels for the profile products represented in $nal$ (nal: number of atmospheric levels) levels, i.e. they are matrices of dimension $nal \times nal$. Logarithmic scale kernels are also called fractional or relative averaging kernels (e.g. Keppens et al., 2015).

Figure 2 depicts the rows of typical averaging kernels for the MUSICA IASI product (panel a) and the combined data product (panel b). Adding the information provided by TROPOMI clearly improves the sensitivity in the lower troposphere: for the MUSICA IASI product the lower tropospheric kernels generally peak at the upper limit of the lower troposphere (at about 5 km a.s.l.). For the combined product these peak values are obtained at significantly lower altitudes (at about 2.5 km a.s.l.). In the upper troposphere/lower stratosphere (UTLS) we see no significant difference between the kernels.

In this work we focus on the total column and the partial columns between the surface and 6 km a.s.l. (the tropospheric partial column) and between 6 km a.s.l. and 20 km a.s.l. (the UTLS partial column). The total and partial column kernels are calculated from $\mathbf{A}_\mathbf{I}^\mathbf{l}$ and $\mathbf{A}_\mathbf{C}^\mathbf{l}$ by their transformation on linear scale (see Appendix B) and the vertical resampling as explained in Appendix C. Figure 3 depicts the total and partial column kernels corresponding to the row kernels of Fig. 2.

Total column amount kernels are available for all three products (see Fig. 3a): the TROPOMI, the MUSICA IASI, and the combined product. The TROPOMI kernel is close to unity for all altitudes, documenting the good sensitivity for $CH_4$ at all altitudes. The combined total column amount kernel is very similar to the respective TROPOMI kernel (even correcting the overshoot at 4-6 km) and means that the combined retrieval product does also well reflect the actual atmospheric total column amounts. The MUSICA IASI kernel has relatively low values in the lower troposphere and above 15 km, only in the UTLS region the kernel values are between 0.75 and 1.25. This means that MUSICA IASI can actually not well detect total column amounts, because it lacks sensitivity in the lower troposphere. The altitude regions where the MUSICA IASI product has

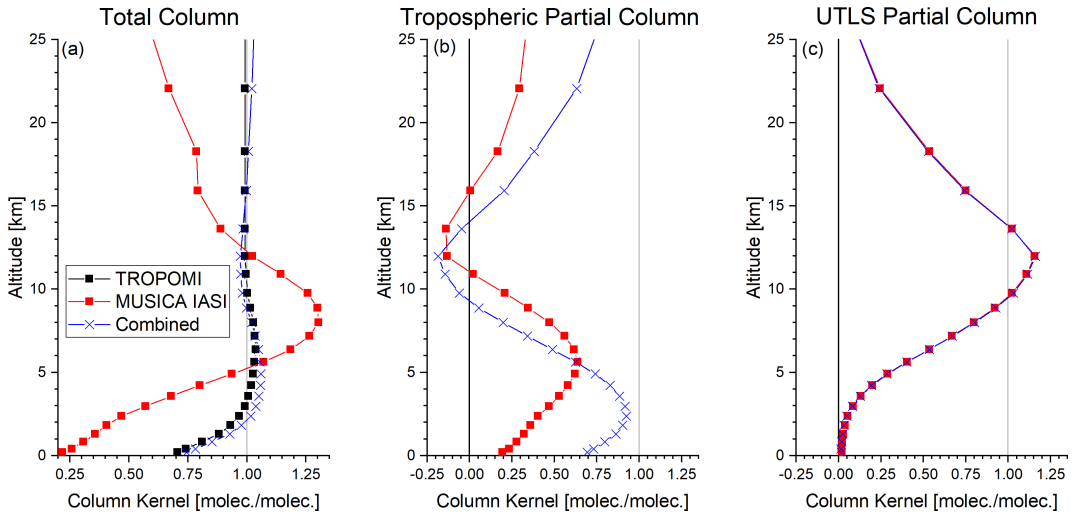


**Figure 3.** Total column amount and partial column amount kernels corresponding to the TROPOMI, MUSICA IASI, and combined product for the same late summer observation as used in Figs. 1 and 2: (a) total column amount kernels; (b) lower tropospheric partial column amount kernels, surface - 6 km a.s.l.; (c) upper tropospheric/lower stratospheric (UTLS) partial column amount kernels, 6 - 20 km a.s.l.

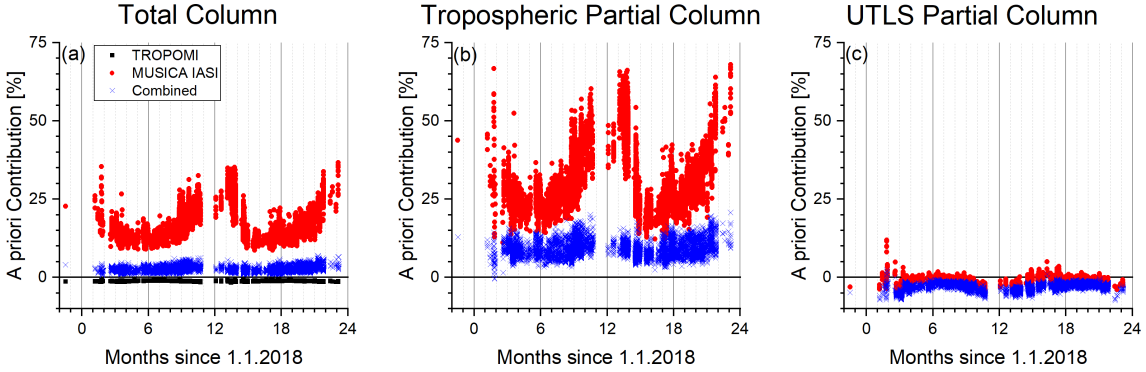


**Figure 4.** Relative contribution of the a priori data to the retrieved products (black squares: TROPOMI, red dots: MUSICA IASI, blue crosses: Combined product): (a) total column; (b) tropospheric partial column; (c) UTLS partial column.

reduced sensitivities are the regions where TROPOMI's total column information has the strongest impact on the combined product (see Fig. 1).

Partial column amount kernels are only available for profile products, i.e. the MUSICA IASI and the combined product (MUSICA IASI updated with information from TROPOMI). Figure 3b shows tropospheric partial column amount kernels. For the MUSICA IASI product we observe values that are generally lower than 0.5. The highest values are achieved around 6 km a.s.l., i.e. at the upper boundary of vertical layer we defined as the tropospheric partial column. The kernel of the combined

product shows a good sensitivity with peak values of almost 0.95 at 2.5 km a.s.l. and values above 0.75 for almost all altitudes between the surface and 6 km a.s.l.

UTLS partial column amount kernels are depicted in Figure 3c. The values are close to unity for most of the altitudes that we attributed to the UTLS layer (altitudes between 6 km and 20 km a.s.l.). There is almost no difference between the MUSICA IASI and the combined kernels, meaning that the information provided by TROPOMI has almost no effect on the UTLS partial column, which is because the MUSICA IASI product is already very sensitive to this altitude region.

According to Eqs. (A1) and (A3) for the MUSICA IASI and combined retrieval data we can write

$$\hat{\boldsymbol{x}}^{\boldsymbol{l}} = \mathbf{A}^{\mathbf{l}}\boldsymbol{x}^{\boldsymbol{l}} + (\mathbf{I} - \mathbf{A}^{\mathbf{l}})\boldsymbol{x}_{\boldsymbol{a}}^{\boldsymbol{l}}, \tag{4}$$

with $\mathbf{I}$ being the identity operator and $\boldsymbol{x}^{\boldsymbol{l}}$ the actual atmospheric state in logarithmnic scale. Equation (4) reveals that the term $(\mathbf{I} - \mathbf{A}^{\mathbf{l}})\boldsymbol{x}_{\boldsymbol{a}}^{\boldsymbol{l}}$ captures the relative contribution of the a priori to the retrieved product. The resampling of this term on total and partial columns is made according to Eq. (C6). For the TROPOMI total column averaged mixing ratios we can calculate the apriori contribution by $(\boldsymbol{w}^{*T} - \boldsymbol{a}_{\boldsymbol{T}}^{*T})\boldsymbol{x}_{\boldsymbol{a}}$. For more details see Appendix C.

Figure 4 depicts the a priori contribution relative to the retrieved values for the total column, the tropospheric and UTLS partial columns. Shown are time series for measurements over Central Europe, which confirm the observations made in the context of the example kernels of Fig. 3: for the total column (Fig. 4a) the a priori contribution on the TROPOMI and the combined products are rather small and can be neglected, i.e. both products can detect total column signals. In contrast the MUSICA IASI total column product is significantly affected by the a priori data, i.e. provides no independent observation of the total column. Concerning partial column products (Fig. 4b and c) we can compare the MUSICA IASI and the combined product (the TROPOMI product has no information on the vertical distribution). The tropospheric MUSICA IASI partial column is significantly affected by the a priori, but the combined product is largely independent on the a priori data. In the UTLS both the MUSICA IASI and combined products are largely independent on the apriori data. In summary, with IASI alone we can well detect signals in the UTLS, but not in the lower troposphere. The detection of signals in both altitude regions independently from the a priori information is only possible by using the combined product.

### 2.4 Retrieval noise error

In this section we compare the retrieval noise errors of the individual retrieval products with those achieved when combining the two retrieval products. According to Eq. (1) we can calculate the retrieval noise covariance matrix for the combined data product by

$$\mathbf{S}_{\hat{\mathbf{x}}_{\mathbf{C}},\mathbf{n}}^{\mathbf{l}} = (\mathbf{I} - \mathbf{L}^{-1}\boldsymbol{m}\boldsymbol{a}_{\boldsymbol{T}}^{*T})\mathbf{L}\mathbf{S}_{\hat{\mathbf{x}}_{\mathbf{I}},\mathbf{n}}^{\mathbf{l}}\mathbf{L}^{T}(\mathbf{I} - \mathbf{L}^{-1}\boldsymbol{m}\boldsymbol{a}_{\boldsymbol{T}}^{*T})^{T} + (\mathbf{L}^{-1}\boldsymbol{m})S_{\hat{x}_T,n}(\mathbf{L}^{-1}\boldsymbol{m})^{T}. \tag{5}$$

Here $\mathbf{S}_{\hat{\mathbf{x}}_{\mathbf{I}},\mathbf{n}}^{\mathbf{l}}$ is the retrieval noise covariance matrix of the MUSICA IASI retrieval. The error covariances resampled to the total and partial columns are then determined according to Appendix C. Figure 5 shows the retrieval noise errors (which are the square root values of the error variances) relative to the retrieved values for the total column and the tropospheric and UTLS partial columns.

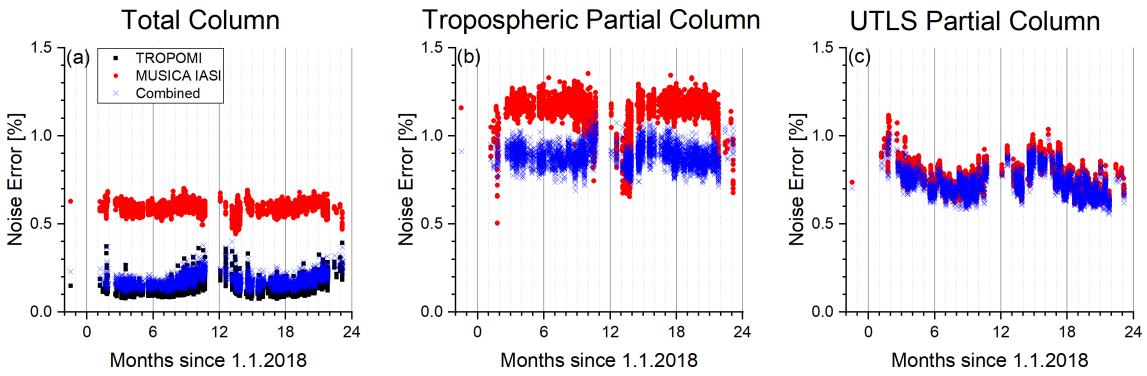


**Figure 5.** Estimated relative noise error for the retrieved products (colours like in Fig. 4): (a) total column; (b) tropospheric partial column; (c) UTLS partial column.

The errors for the total columns (Fig. 5a) are generally below 0.2% for the TROPOMI product. For the MUSICA IASI product they are rather stable at about 0.6%. Concerning the combined product the retrieval noise error is very similar to the retrieval noise error of the TROPOMI data.

For the tropospheric partial columns (Fig. 5b) the error is in general above 1% for the MUSICA IASI product and below 1% for the combined product. For the UTLS partial columns (Fig. 5c) we observe an error of generally below 1% and no significant difference between the MUSICA IASI and the combined data products. This suggests that the error in the combined product is dominated by the error in the MUSICA IASI data, which reveals the very limited impact of the TROPOMI data on the combined UTLS data product.

## 3 Validation

In this section we compare the TROPOMI, MUSICA IASI, and combined products to different reference data products. As reference for the total column averaged mixing ratio ($XCH_4$) we use TCCON (Total Carbon Column Observing Network, Wunch et al., 2011) ground-based remote sensing data from five sites located in different climate zones. As reference for the total and the partial columns we use in-situ profiles measured by the AirCore system (Karion et al., 2010) at two geophysically different European locations. Furthermore, we use in-situ data measured at two nearby Central European Global Atmospheric Watch (GAW) mountain stations.

Figure 6 depicts the geographical location of the European reference observations. We consider the European TCCON stations at Sodankylä (Finland) and Karlsruhe (Germany). They are indicated as red crosses together with a circle around the stations with a radius of 150 km indicating the spatial collocation criteria: only satellite observations with ground pixels inside this circle are compared to the TCCON data. Blue crosses and circles represent the locations of AirCore measurements (at Trainou, France, and Sodankylä, Finland) and their spatial collocation criteria, respectively. Here we relax the radius of the collocation circle to 500 km in order to achieve a sufficient high number of coincidences between AirCore and satellite

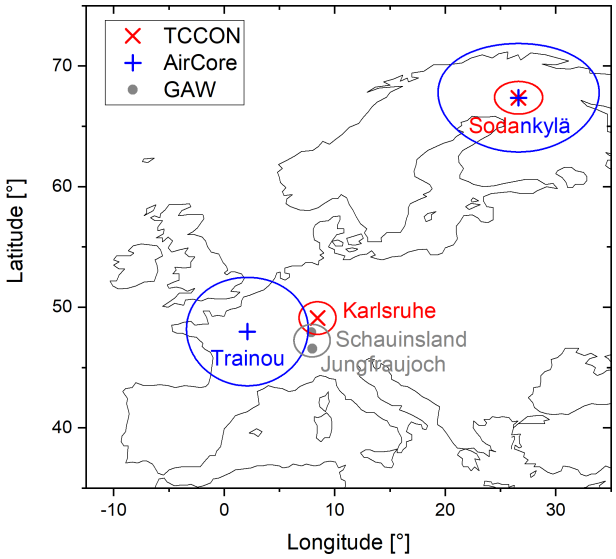


**Figure 6.** Map showing the location of the European reference measurements and the areas accepted for valid horizontal collocation. Blue crosses and circles: sites with AirCore measurements and circles with 500 km radius. Red crosses and grey dots: sites with TCCON and GAW measurements, respectively, and circles with 150 km radius.

observations. The two grey dots indicate the locations of the two GAW stations (Jungfraujoch in Switzerland and Schauinsland in South-western Germany) and the respective grey spatial collocations circle around the middle distance point of the two stations has a radius of 150 km.

### 3.1 TCCON $XCH_4$

We use TCCON ground-based remote sensing data from six exemplary sites located in different climate zones representative for high, mid and low latitudes. The Sodankylä site is located at high latitudes, Karlsruhe and Lauder are located in the northern and southern hemispheric mid-latitudes, Wollongong is located in the subtropics, and Burgos and Darwin are located in the tropics. More details on locations of these sites and references for the used data sets are given in Table 1.

We use the TROPOMI a priori setting for the comparison between the ground-based TCCON and the satellite-based remote sensing products. For this purpose the TCCON product is adjusted to the TROPOMI a priori settings according to Eq. (A16), which ensures the usage of the same a priori data for all the remote sensing products. As spatial collocation criteria we require that the ground pixels of the TROPOMI and the IASI measurement fall within a circle with a radius of 150 km around the TCCON sites. For collocation with respect to time, TCCON, TROPOMI, and IASI observations have to be made within at least 6 hours. Furthermore, we require that the altitude differences between the TCCON stations and the satellite ground pixels are within 250 m.

We estimate the reliability of the TCCON data as reference for the satellite observations. For this estimation we consider the TCCON retrieval noise errors, the incomparableness of TCCON and satellite data caused by their different averaging kernels,

**Table 1.** Locations of TCCON sites used in this study and references for the used TCCON data sets.

| Name and Country | Latitude | Longitude | Altitude | Reference |
|---|---|---|---|---|
| Sodankylä, Finland | 67.4°N | 26.6°E | 190 m a.s.l . | Kivi et al. (2014); Kivi and Heikkinen (2016) |
| Karlsruhe, Germany | 49.1°N | 8.4°E | 120 m a.s.l. | Hase et al. (2015) |
| Burgos, Philippines | 18.5°N | 120.7°E | 40 m a.s.l. | Velazco et al. (2017) |
| Darwin, Australia | 12.5°S | 130.9°E | 40 m a.s.l. | Griffith et al. (2014a) |
| Wollongong, Australia | 34.4°S | 150.9°E | 30 m a.s.l. | Griffith et al. (2014b) |
| Lauder, New Zealand | 45.0°S | 169.7°E | 610 m a.s.l. | Sherlock et al. (2014); Pollard et al. (2019) |

and the collocation mismatch. The total column uncertainty variance (the scalar $S_{\mathrm{ref}}$) for using the TCCON data as reference for the satellite data can be estimated by:

$$S_{\mathrm{ref}} = S_{\Delta\mathrm{TC}} + (\boldsymbol{a}^{*T} - \boldsymbol{a}^{*}_{\mathbf{TC}}{}^{T})\mathbf{S}_{\mathbf{\Delta a}}(\boldsymbol{a}^{*T} - \boldsymbol{a}^{*}_{\mathbf{TC}}{}^{T})^{T} + \boldsymbol{a}^{*}_{\mathbf{TC}}{}^{T}(\mathbf{S}_{\mathbf{\Delta}_{\mathrm{t}}} + \mathbf{S}_{\mathbf{\Delta}_{\mathrm{h}}})\boldsymbol{a}^{*}_{\mathbf{TC}}, \tag{6}$$

The first term (the scalar $S_{\Delta\mathrm{TC}}$) is the TCCON retrieval error covariance (the TCCON error is provided with the TCCON data is typically 1‰). The second term accounts for the different averaging kernels. The row vectors $\boldsymbol{a}^{*T}$ and $\boldsymbol{a}^{*}_{\mathbf{TC}}{}^{T}$ are the total column averaged mixing ratio kernels of the satellite and the TCCON retrievals, respectively (calculated according to Appendix C). The matrix $\mathbf{S}_{\mathbf{\Delta a}}$ describes the uncertainty covariances of the used a priori data. We determine these uncertainty covariances from the TM5 $CH_4$ simulations (Krol et al., 2005), which are provided in the TROPOMI data set as the a priori data. For this purpose we assume a hypothetical out-of-phase of the model of 24 hours and in addition a horizontal mismatch of the modeled $CH_4$ fields of 500 km. The covariances obtained for the differences between the original TM5 model fields and the TM5 fields with the hypothetical model deficits are then used as the uncertainty covariances. We found an a priori uncertainty covariance $\mathbf{S}_{\mathbf{\Delta a}}$ having largest values close to the surface but even there, the uncertainty variance is smaller than $(4‰)^2$. Due to this good a priori knowledge the effect of the different averaging kernels on the comparison is less than 0.5‰ (even for the comprison between the TCCON and the MUSICA IASI products, where the difference in the averaging kernels is most significant). The third term takes into account that TCCON and the satellites might detect different air masses. The respective uncertainty covariances are again estimated with the TM5 $CH_4$ simulations. We determine the covariances between out-of-phase model fields and the correct model fields for different out-of-phase time intervals. Similarly we calculate the covariances between model fields that have a horizontal mismatch and the correct model fields for different horizontal mismatch intervals. The temporal collocation uncertainty covariance ($\mathbf{S}_{\mathbf{\Delta}_{\mathrm{t}}}$) and the horizontal collocation uncertainty covariance ($\mathbf{S}_{\mathbf{\Delta}_{\mathrm{h}}}$) are then the covariances interpolated to the actual temporal and horizontal mismatch of the satellite and the TCCON measurements. The effect of this collocation mismatch on the comparison of the total columns is estimated to be smaller than 0.5‰. In summary, we estimate the reliability of the TCCON data as reference for the satellite total column observations to be within 2‰.

12-1

In Fig. 7 the TROPOMI, MUSICA IASI, and combined $XCH_4$ products are compared to the TCCON $XCH_4$ data. The crosses represent the daily mean data and the filled symbols in the background show all data corresponding to all individual

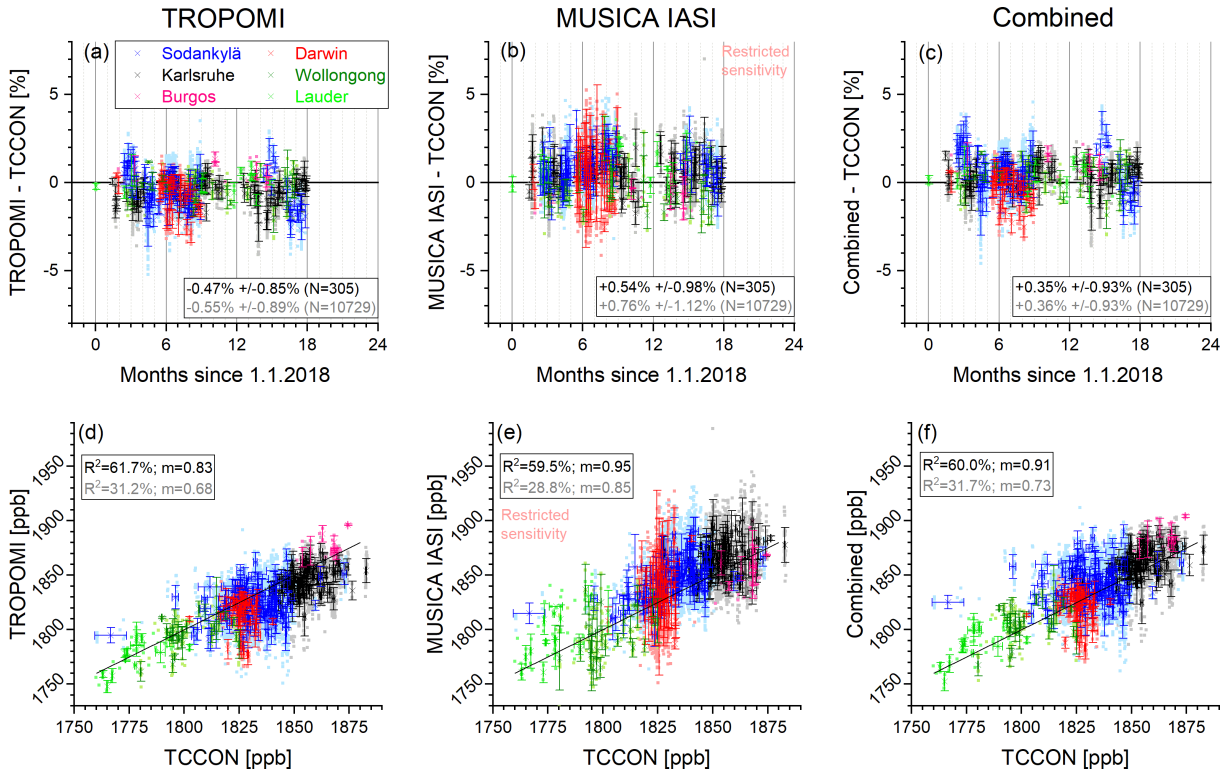


**Figure 7.** Comparison of the different $XCH_4$ satellite products with TCCON $XCH_4$ data from five globally representative stations (the different colours correspond to the stations as given in the legend). Data for all individual coincidences are plotted in the background as squares and daily mean data are depicted as crosses with error bars representing the $1\sigma$ standard deviation: (a)-(c) shows time series of the differences, text in dark and pale fonts report mean and $1\sigma$ standard deviation (scatter) determined from daily mean data and from all individual collocations, respectively; (d)-(f) visualises the correlations (the black line is the one-to-one diagonal), text in dark and pale fonts report coefficients of determination ($R^2$) and the slope of the linear regression line ($m$) obtained for a linear least squares fit on daily mean data and on data from all individual collocations, respectively.

valid collocations. Figure 7a-c show time series of the differences with respect to the TCCON references. The daily mean data have error bars, which is the $1\sigma$ standard deviation of the data used for calculating the daily mean.

Statistics in form of mean difference and $1\sigma$ $1\sigma$ standard devation (scatter) around the mean difference are given in each panel (for statistics using daily mean data in black fonts and for statistics using all individual valid collocations in grey fonts). Concerning TROPOMI (Fig. 7a) we observe – in line with Lorente et al. (2020) – a very good agreement. For daily mean data as well as for the statistics based on all individual differences, the mean difference is within 0.55% and the scatter lies below 1%. A very good agreement and low values for mean difference and scatter are also achieved for the combined product (Fig. 7c). For the MUSICA IASI product (Fig. 7b) we have reduced sensitivity in the lower troposphere (see Figs. 3 and 4) and the observed good agreement with the TCCON $XCH_4$ data can be partly explained by the reliable a priori data.

Figure 7d-f depicts correlation plots. For daily mean data the coefficients of determination ($R^2$) are about 58% for the TROPOMI product and about 55% for the combined product. When considering all individual coincidences the $R^2$ values are almost 30%. The error bars on the daily mean data are the $1\sigma$ standard deviations of the data used for calculating the daily mean. For the MUSICA IASI product, we observe a similar good correlation than for the TROPOMI and the combined products. However, concerning the MUSICA IASI data part of the common signal might be due to the a priori on which the MUSICA IASI total column product is not independent (see Fig. 4a).

4-1

4-2

The satellite $XCH_4$ data show a very good agreemet with the TCCON data. Considering the estimated reference reliability of the TCCON data of about 2‰ we are not able to identify any bias in the satellite data.

### 3.2 Air-Core in-situ $CH_4$ profiles

We use the AirCore balloon borne in-situ measurements (Karion et al., 2010) as the reference for $CH_4$ total columns as well as for the $CH_4$ vertical distribution. The AirCore system samples the vertical distribution of $CH_4$ with a much better vertical resolution than the satellite remote sensing systems. For this reason we can generate an AirCore profile ($\hat{\boldsymbol{x}}_{\mathrm{AC}}$) that has the same vertical sensitivity and resolution characteristics as the remote sensing data. According to Eqs. (A1) and (A3) for the MUSICA IASI and the combined retrieval data we can write:

$$\hat{\boldsymbol{x}}^{\boldsymbol{l}}{}_{\mathrm{AC}} = \boldsymbol{x}^{\boldsymbol{l}}_{\boldsymbol{a}} + \mathbf{A}^{\mathbf{l}}(\boldsymbol{x}^{\boldsymbol{l}}{}_{\mathrm{AC}} - \boldsymbol{x}^{\boldsymbol{l}}_{\boldsymbol{a}}). \tag{7}$$

Here $\mathbf{A}^{\mathbf{l}}$ and $\boldsymbol{x}^{\boldsymbol{l}}_{\boldsymbol{a}}$ are the logarithmic scale averaging kernels and the logarithmic scale a priori state of the satellite retrieval, respectively, $\boldsymbol{x}^{\boldsymbol{l}}{}_{\mathrm{AC}}$ is the measured logarithmic scale AirCore profile regridded to the atmospheric model grid used for the satellite retrievals. The resampling of these data on total and partial columns is made with the linear scale data according to Eq. (C6). For the TROPOMI total column averaged mixing ratios we calcuated the adjusted AirCore total column averaged mixing ratio (a scalar) by $\hat{x}_{\mathrm{AC}} = \boldsymbol{w}^{*T}\boldsymbol{x}_{\boldsymbol{a}} + \boldsymbol{a}^{*}_{\boldsymbol{T}}{}^{T}(\boldsymbol{x}_{\mathrm{AC}} - \boldsymbol{x}_{\boldsymbol{a}})$. For more details see Appendix C.

As spatial collocation criteria we require that the ground pixels of the TROPOMI and the IASI measurement fall within a circle with a radius of 500 km around the mean horizontal location of the AirCore system when sampling between the 450 and 550 hPa pressure levels. The temporal collocation is 6 hours. AirCore data are typically not available close to the ground and above the burst altitude of the balloon (approximately 25 hPa). At low altitudes we extend the profile with the concentrations closest to the ground. At high altitudes we extend the profile with the TM5 model data, with a smooth transition between the measured values and the modelled data.

Similar to the TCCON data we estimate the reliability of the AirCore profile data as reference for the satellite observations. For this estimation we consider an AirCore measurement noise covariance ($\mathbf{S}_{\boldsymbol{\Delta}\mathrm{AC,n}}$). It is calculated assuming an uncertainty for altitudes with AirCore $CH_4$ data of 0.3% (Karion et al., 2010) and the uncertainty according to $\mathbf{S}_{\boldsymbol{\Delta}\mathbf{a}}$ from Sect.3.1 for all other altitudes. The outer diagonal elements are determined by assuming the same vertical correlation as derived for $\mathbf{S}_{\boldsymbol{\Delta}\mathbf{a}}$. In addition, we consider uncertainties in the height attribution, which is according to Wagenhäuser et al. (2021) below 10 m close to ground, about 200 m at 20 km a.s.l. and about 1 km at 27 km a.s.l. For some AirCore soundings there was a problem with the electronic board. For those measurements information on pressure, altitude and temperature had to be reconstructed

from the radiosonde data and we use for all altitude levels an additional height attribution uncertainty value of 500 m. We construct a respective height attribution uncertainty covariance ($\mathbf{S}_{\mathbf{\Delta}\mathrm{AC,v}}$) by assuming a very strong correlation of the height attribution uncertainties between different altitude levels. The temporal and spatial collocation uncertainty covariance between the AirCore and the satellite observations ($\mathbf{S}_{\mathbf{\Delta}\mathrm{t}}$ and $\mathbf{S}_{\mathbf{\Delta}\mathrm{h}}$, respectively) are calculated as described in Sect. 3.1.

All the aforementioned uncertainties are independent and we can calculate the total uncertainty as:

$$\mathbf{S}_{\mathbf{\Delta}\mathrm{AC}} = \mathbf{S}_{\mathbf{\Delta}\mathrm{AC,n}} + \mathbf{S}_{\mathbf{\Delta}\mathrm{AC,v}} + \mathbf{S}_{\mathbf{\Delta}\mathrm{t}} + \mathbf{S}_{\mathbf{\Delta}\mathrm{h}}. \tag{8}$$

The reliability of the AirCore data – after its adjustment according to Eq. (7) – as reference for the MUSICA IASI and combined satellite data can then be estimated by:

$$\mathbf{S}^{\mathbf{l}}_{\mathrm{ref}} = \mathbf{A}^{\mathbf{l}}\mathbf{S}^{\mathbf{l}}_{\mathbf{\Delta}\mathrm{AC}}\mathbf{A}^{\mathbf{l}^T}. \tag{9}$$

Here and in Eq. (8) the covariances are determined for the full vertical profile. Respective covariances for total or partial columns can be derived according to Appendix C. The reliability for the TROPOMI total column averaged mixing ratio data can be calculated by $S_{\mathrm{ref}} = \boldsymbol{a}^{*\,T}_{\boldsymbol{T}}\mathbf{S}_{\mathbf{\Delta}\mathrm{AC}}\boldsymbol{a}^{*}_{\boldsymbol{T}}$.

Table 2 gives an overview on the AirCore profiles measured at Trainou (France, 48.0°N, 2.1°E) and Sodankylä (Finland, 67.4°N, 26.6°E). In total we have 24 individual AirCore profiles with collocated satellite observations. The total number of collocated satellite observations is 5308. We estimate that the AirCore data can serve as reliable references for the satellite data validation. The three columns on the right report the uncertainties determined according to Eq. (8). For the reliability – according to Eq. (9) – we get very similar values (exept for the total column and the partial tropospheric column of the MUSICA IASI product, because of the limited sensitivity). It is 3-6‰, 3-5‰, and 3-7‰, for the total column, the tropospheric partial column and the UTLS partial column, respectively. In the troposphere the reliability depends mainly on the availability of AirCore data close to the ground and in the UTLS uncertainties of the altitude attribution have a dominating influence.

The comparison between the TROPOMI and the AirCore $XCH_4$ data is shown in Fig. 8. The differences of collocated measurements are shown in Fig. 8a. The agreement between TROPOMI and AirCore is very good and the mean difference and the $1\sigma$ sigma standard deviation (scatter) around the mean difference is similar to the comparison between TROPOMI and TCCON. Considering the mean values for all coincidences corresponding to the same AirCore flight, we observe a coefficient of determinarion ($R^2$) of about 31%. This is lower than the $R^2$ value achieved for the correlation with TCCON data; however, we have to consider that the amplitude in the analysed total column signals is much smaller in the AirCore data set if compared to the TCCON data set.

15-1

15-2

Figure 9 presents the comparison between the MUSICA IASI and AirCore total column and tropospheric and UTLS partial column data. The differences between both data sets are depicted in Fig. 9a-c. We find a very good agreement for the UTLS partial column data (mean difference of about 0.6% and a scatter of 1%). Because at this altitude region the MUSICA IASI product is almost independent from the a priori assumption (see Sect. 2.3), the a priori effect on $\hat{\boldsymbol{x}}_{\mathrm{AC}}$ from Eq. 7 can also be neglected and we compare here two independent data sets. For the total column we also see a good agreement (Fig. 9a). However according to Sect. 2.3 the MUSICA IASI total column products are significantly affected by the a priori data and so is $\hat{\boldsymbol{x}}_{\mathrm{AC}}$ from Eq. 7, i.e. here we actually do not compare two independent data sets and a significant part of the good agreement

**Table 2.** List with information about the AirCore flights. [$P_{\min}$,$P_{\max}$] is the pressure range covered by the AirCore measurements. $N$ is the number of collocated satellite observations (one collocation of IASI and TROPOMI counts as one). $P_{\max} = \overline{P_{\mathrm{GND}}^{\mathrm{Sat.}}} - P_{\max}$ is the mean difference between AirCore maximum pressure value and the pressure values for the collocated satellite ground pixels. $\overline{\Delta h}$ is the mean horizontal distance between the AirCore system (location for AirCore system at 450-550 hPa) and the locations of the satellite ground pixels. $\overline{\Delta t} = \overline{t^{\mathrm{Sat.}}} - t$ is the mean time difference between the AirCore observations (time for AirCore system at 450-550 hPa) and the satellite observations. $\overline{\Delta \mathrm{AC}_{\mathrm{tot}}}$, $\overline{\Delta \mathrm{AC}_{\mathrm{tro}}}$, and $\overline{\Delta \mathrm{AC}_{\mathrm{utls}}}$ are the square roots of the variances (determined according to Eq. (8) and the column calculations according to Appendix C). These are the estimated uncertainties for using the adjusted AirCore data as reference for the satellite data: for the total column (index: 'tot') and the tropospheric and UTLS partial columns (indices 'tro' and 'utls', respectively).

| ID | Location | Date | $P_{\min}$ | $P_{\max}$ | $N$ | $\overline{\Delta P_{\max}}$ | $\overline{\Delta h}$ | $\overline{\Delta t}$ | $\overline{\Delta \mathrm{AC}_{\mathrm{tot}}}$ | $\overline{\Delta \mathrm{AC}_{\mathrm{tro}}}$ | $\overline{\Delta \mathrm{AC}_{\mathrm{utls}}}$ |
|---|---|---|---|---|---|---|---|---|---|---|---|
| | | [YYYYMMDD] | [hPa] | [hPa] | | [hPa] | [km] | [min] | [%] | [%] | [%] |
| 0-1 | Trainou | 20180523 | 29.0 | 962.3 | 68 | +43.4 | 409 | -41 | 0.4 | 0.4 | 0.4 |
| 1-2 | | 20180525 | 26.4 | 972.2 | 21 | -0.4 | 361 | -47 | 0.3 | 0.4 | 0.3 |
| 2-3 | | 20190220 | 21.9 | 983.4 | 241 | +14.3 | 302 | -76 | 0.6 | 0.5 | 0.7 |
| 3-4 | | 20190220 | 19.2 | 940.5 | 184 | +58.5 | 304 | -138 | 0.3 | 0.4 | 0.3 |
| 4-5 | | 20190221 | 19.8 | 902.7 | 410 | +93.4 | 279 | -76 | 0.6 | 0.5 | 0.7 |
| 5-6 | | 20190221 | 19.4 | 986.3 | 327 | +11.6 | 273 | -117 | 0.3 | 0.4 | 0.4 |
| 6-7 | | 20190617 | 20.5 | 910.9 | 375 | +64.8 | 355 | -227 | 0.5 | 0.4 | 0.6 |
| 7-8 | | 20190618 | 23.8 | 972.8 | 31 | +66.8 | 375 | -104 | 0.6 | 0.5 | 0.7 |
| 8-9 | | 20190621 | 44.6 | 869.1 | 2 | +141.6 | 216 | -47 | 0.6 | 0.5 | 0.6 |
| 9-10 | | 20191011 | 38.1 | 914.8 | 282 | +64.8 | 314 | -81 | 0.5 | 0.5 | 0.6 |
| 10-11 | Sodankylä | 20180417 | 19.8 | 963.9 | 13 | +17.9 | 249 | -140 | 0.3 | 0.3 | 0.4 |
| 11-12 | | 20180528 | 36.3 | 959.1 | 167 | +43.3 | 401 | +9 | 0.3 | 0.3 | 0.4 |
| 12-13 | | 20180618 | 32.9 | 937.5 | 12 | +57.2 | 411 | -39 | 0.3 | 0.3 | 0.4 |
| 13-14 | | 20180620 | 19.7 | 929.7 | 5 | +66.4 | 316 | -106 | 0.3 | 0.3 | 0.4 |
| 14-15 | | 20180625 | 24.3 | 935.1 | 59 | +66.8 | 357 | -98 | 0.3 | 0.3 | 0.4 |
| 15-16 | | 20180702 | 78.2 | 952.0 | 1166 | +34.0 | 279 | -127 | 0.3 | 0.3 | 0.3 |
| 16-17 | | 20180801 | 15.8 | 962.6 | 454 | +31.7 | 304 | -203 | 0.5 | 0.4 | 0.6 |
| 17-18 | | 20181003 | 13.0 | 916.5 | 1 | +64.9 | 433 | +61 | 0.3 | 0.3 | 0.4 |
| 18-19 | | 20190410 | 15.1 | 975.7 | 51 | +24.3 | 282 | +39 | 0.3 | 0.3 | 0.4 |
| 19-20 | | 20190628 | 16.6 | 952.8 | 18 | +53.5 | 343 | -9 | 0.3 | 0.3 | 0.4 |
| 20-21 | | 20190724 | 16.8 | 961.1 | 206 | +34.7 | 323 | -13 | 0.5 | 0.4 | 0.6 |
| 21-22 | | 20190801 | 16.3 | 957.8 | 10 | +28.1 | 313 | -14 | 0.3 | 0.3 | 0.3 |
| 22-23 | | 20190828 | 13.8 | 966.1 | 679 | +22.4 | 258 | +9 | 0.3 | 0.3 | 0.3 |
| 23-24 | | 20190909 | 24.0 | 968.0 | 161 | +28.9 | 226 | -43 | 0.3 | 0.3 | 0.3 |

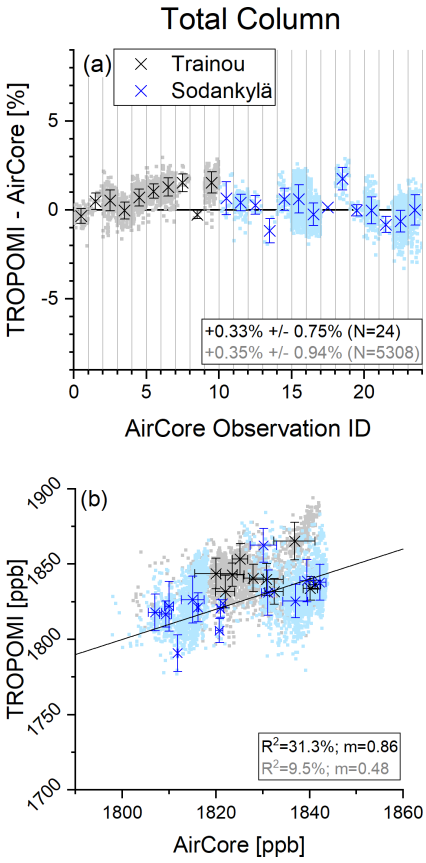


**Figure 8.** Comparison of AirCore measurements made at Trainou (black) and Sodankylä (blue) with the TROPOMI $XCH_4$ product. Data for all individual coincidences are shown in the background as squares and averages per flight are depicted as crosses with error bars representing the estimated uncertainty: (a) shows the series of differences ordered by flight number, text in dark and pale fonts report mean and $1\sigma$ standard deviation (scatter) determined from the averages per flight and from all individual collocations, respectively; (b) visualises the correlation (the black line is the one-to-one diagonal), text in dark and pale fonts report coefficients of determination ($R^2$) and the slope of the linear regression line ($m$) obtained for a linear least squares fit on the averages per flight and on all individual collocations, respectively. Details about the corresponding AirCore flights are provided in Table 2.

might be due to the common a priori effect. For the tropospheric partial columns (Fig. 9b) the agreement worsens a bit. We get a mean difference of about 2.4% and a scatter around the mean differences of about 1.3%. The increased mean difference might indicate a systematic bias in the MUSICA IASI lower tropospheric partial columns, which might also explain the increased scatter: the bias will depend on the actual sensitivity of the MUSICA IASI product, which in turn varies with the conditions present during the observation (mainly the surface temperature and the vertical temperature and humidity profiles).

Figure 9d-f shows respective correlation plots. We get very high $R^2$ values for the UTLS partial column, where the two data sets are largly independent (almost not affected by the a priori data). This demonstrates that the MUSICA IASI product

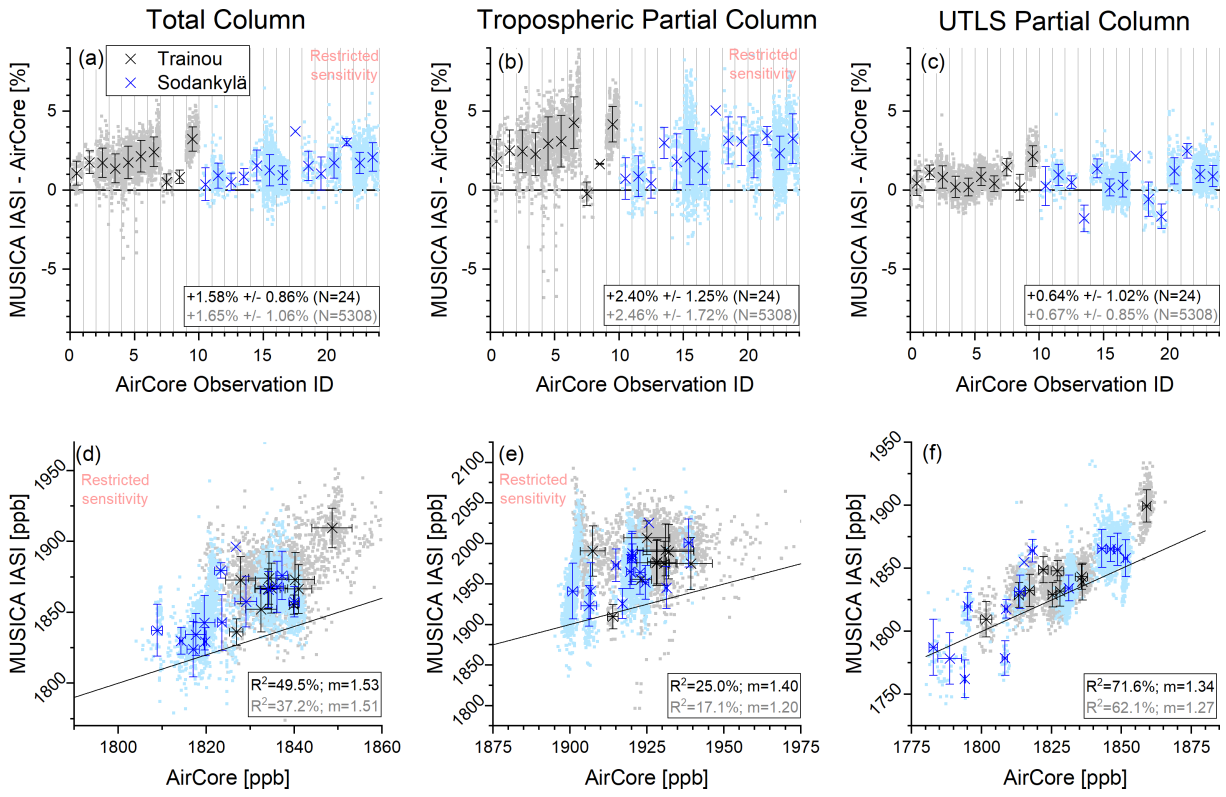


**Figure 9.** Same as Fig. 8, but for comparisons with the MUSICA IASI $XCH_4$, tropospheric $CH_4$, and UTLS $CH_4$ products: (a)-(c) shows the series of differences order by flight number; (d)-(f) visualises the correlation.

reliably captures the actual atmospheric $CH_4$ signals in the UTLS. Concerning the total column and the tropospheric partial column the MUSICA IASI and the adjusted AirCore data are not independent, neverthless the $R^2$ values are lower than for the UTLS partial coloumns. This is due to a low amplitude of the respective signals (total column) and due to varying MUSICA IASI sensitivities, which causes a varying impact of a possible systematic bias (tropospheric partial column).

All combined products (total column and tropospheric and UTLS partial columns) are practically independent from the a priori assumptions (see Fig. 4). Figure 10a-c illustrates the differences between AirCore data and the combined products. For the total column we achieve values for the scatter that are similar to the comparison of the respective TROPOMI product. However, we observe a mean difference that is outside the $1\sigma$ scatter and also outside the uncertainty estimated for the AirCore references (see Table 2), which might indicate to a positive bias in the total columns of the combined data product. For the tropospheric partial column we observe a low scatter, but also mean difference of about 1.7% that is outside the $1\sigma$ scatter and outside the AirCore data uncertainty. For the UTLS partial column the mean difference and scatter values are similar to the comparison of the respective MUSICA IASI product.

18-1

The correlation plots (Fig. 10d-f) allow similar conclusions: the combined product can capture total column signals as reliable as the TROPOMI product (apart from a possible weak bias) and UTLS partial columns signals as reliable as the

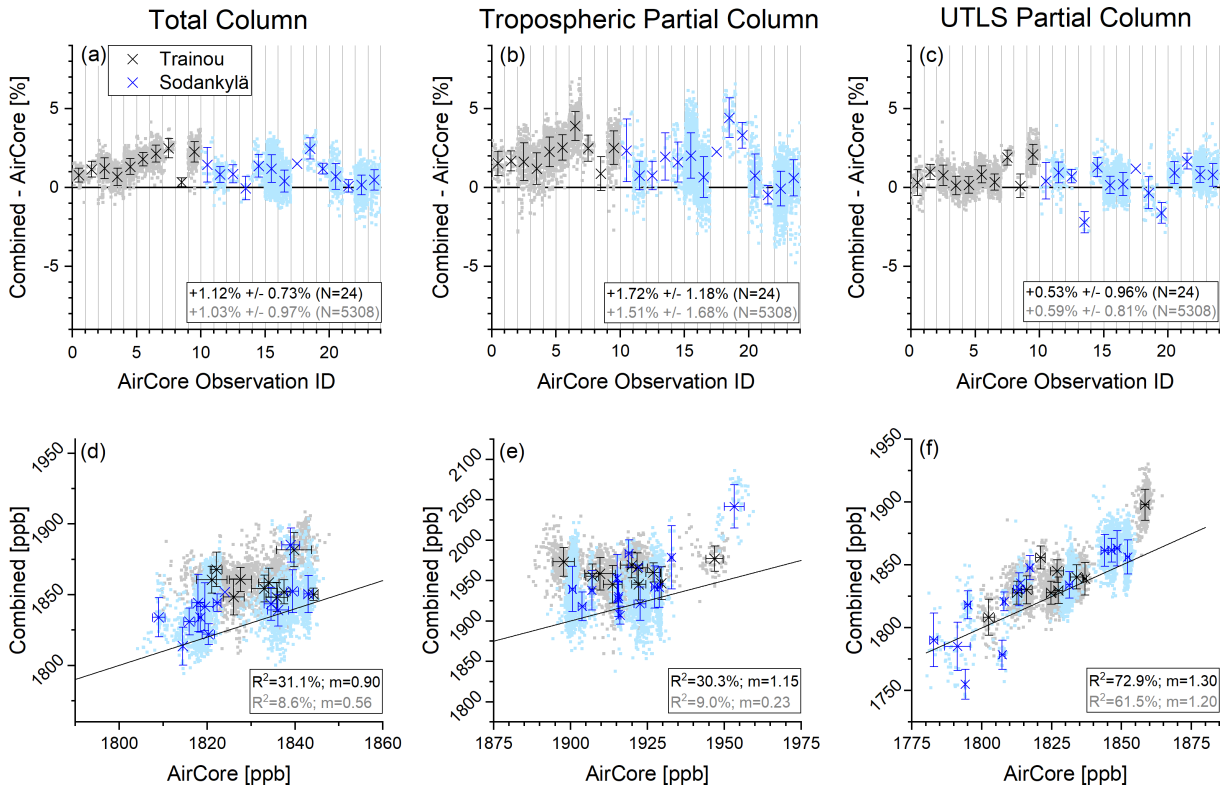


**Figure 10.** Same as Fig. 9, but for comparisons with the combined data products.

MUSICA IASI product. Concerning the tropospheric partial column we observe higher $R^2$ values than for the respective correlation with MUSICA IASI data; however, only when correlating the mean values for all coincidences corresponding to the same AirCore flight. When correlating all individual coincidences the $R^2$ values are even lower than the already low $R^2$ values achieved for the respective correlation with MUSICA IASI data (compare Fig. 9e with Fig. 10e). The low values for $R^2$ are explained by the low $CH_4$ variability encountered during the 24 individual AirCore profiles.

### 3.3 GAW surface in-situ $CH_4$ measurements

At many globally distributed sites atmospheric trace gas in-situ measurements are made continuously with the Global Atmospheric Watch (GAW, https://community.wmo.int/activity-areas/gaw) programme. Appendix A of Sepúlveda et al. (2014) presents a method for filtering common signals in night time $CH_4$ data of the two nearby mountain GAW stations Jungfraujoch (46.5°N, 8.0°E, 3580 m a.s.l.) and Schauinsland (47.9°N, 7.9°E, 1205 m a.s.l.). Data were retained as common signals when deviations of observations (after correction for vertical gradient, i.e. application of an offset, and a temporal shift in the annual cycles) at both sites were below a certain threshold. Sepúlveda et al. (2014) showed that the common signals are well representative for a broader layer in the lower free troposphere. Here we follow this approach and use the mean of the

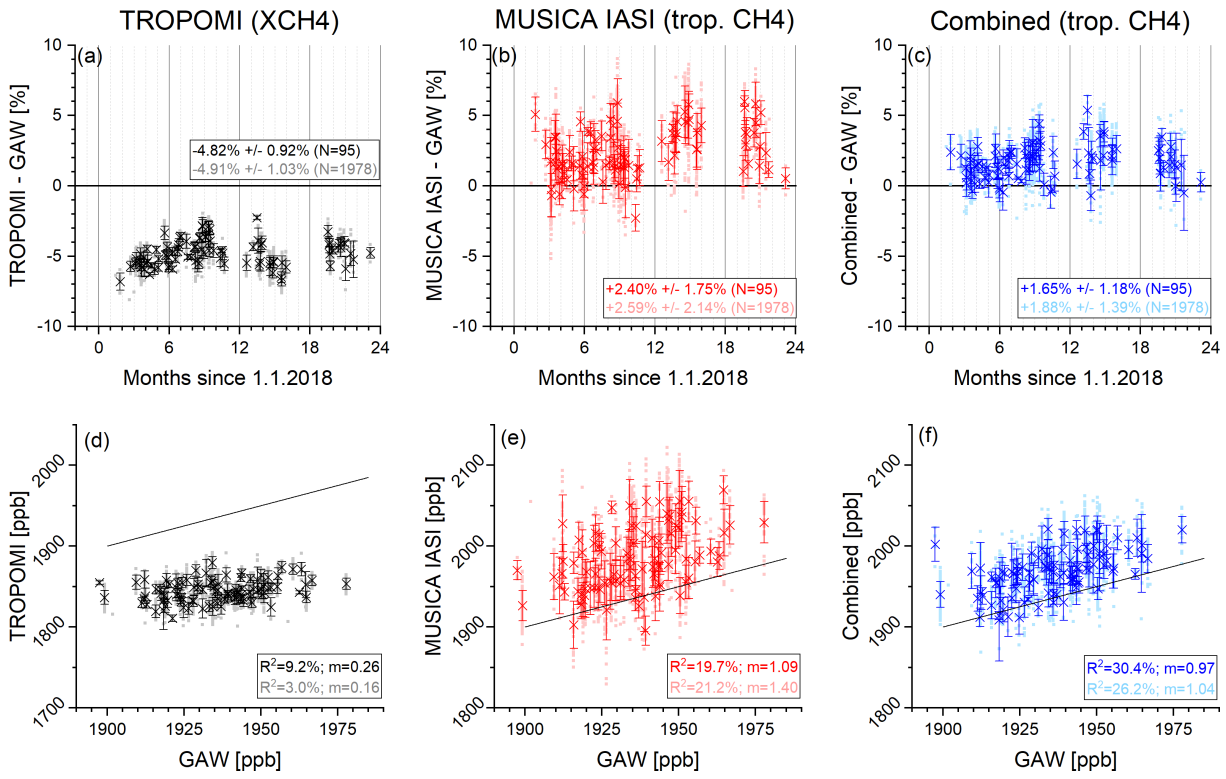


**Figure 11.** Comparison of GAW measurements made at Jungfraujoch and Schauinsland with the TROPOMI $XCH_4$, the IASI tropospheric $CH_4$, and the Combined tropospheric $CH_4$ product. Data for all individual coincidences are shown in the background as squares and daily averages are depicted as crosses with error bars representing the estimated uncertainty: (a)-(c) shows the time series of differences, text in dark and pale coloured fonts report mean and $1\sigma$ standard deviation (scatter) determined from daily mean data and from all individual collocations, respectively; (d)-(f) visualises the correlation (the black line is the one-to-one diagonal), text in normal and bright coloured fonts report coefficients of determination ($R^2$) and the slope of the linear regression line ($m$) obtained for a linear least squares fit on daily mean data and on data from all individual collocations, respectively.

Jungfraujoch and Schauinsland $CH_4$ mixing ratio – whenever identified as a common signal – as a validation reference for the remote sensing data in South-western Germany and Northern Switzerland (indicated by the grey circle in Fig. 6). We assume that the signals obtained from this GAW data filtering are well representative for the tropospheric partial column averaged mixing ratios (surface - 6 km a.s.l.).

Figure 11 shows the comparison with the different satellite products. Concerning the comparison with TROPOMI $XCH_4$ data we observe a very large systematic difference and very low values for $R^2$ (Fig. 11a and d). This indicates that the total column ($XCH_4$) signals are not a good proxy for lower tropospheric $CH_4$ signals, instead the former are strongly affected by signals in the UTLS, where $CH_4$ values are strongly affected by shifts of the tropopause height.

For the MUSICA IASI tropospheric partial column averaged mixing ratio product (Fig. 11b and e) we observe a reduced mean difference than for the TROPOMI $XCH_4$ comparison, but at the same time an increased $1\sigma$ standard deviation (scatter) around the mean. The $R^2$ values are larger than for the correlation of TROPOMI data; however, we have to be careful, because the lower tropospheric MUSICA IASI $CH_4$ data are significantly affected by the a priori assumptions (see Fig. 4b). This means that the observed correlation might actually be due to a correlation with the a priori data.

The combined tropospheric partial column averaged mixing ratio product is practically independent from the a priori assumptions (see Fig. 4b). The good agreement and correlation between the GAW data and the combined products as illustrated in Fig. 11c and f demonstrates that the combined product can reliably capture actual tropospheric $CH_4$ signals independently from the UTLS $CH_4$ signals. For daily mean data we find a mean difference of about 1.7%, a $1\sigma$ scatter of about 1.2%, and an $R^2$ value of almost 30%.

## 4 Summary and outlook

We present a method for a synergetic use of TROPOMI total column and IASI vertical profile retrieval products. The method is based on simple linear algebra calculations, i.e. the execution of computationally expensive dedicated combined retrievals is not needed. Nevertheless, it approximates closely to a dedicated combined optimal estimation retrieval using the combined TROPOMI and IASI measurements (see Appendix A2). We apply the method to $CH_4$ data. By providing a compilation with all important equations we support the application of this method to other data products.

We theoretically examine the sensitivity, vertical resolution, and errors of the individual TROPOMI and IASI products and of the combined product. The TROPOMI product consists of reliable total column $CH_4$ data, but does not offer information on the vertical distribution. The IASI product offers some information on the vertical distribution and has best sensitivity in the UTLS region, but lacks sensitivity in the lower troposphere, i.e. it is not well sensitive to the total column. We show that the combined product combines both strengths: it is a reliable reference for the total column and also for the UTLS partial column. In addition, we found as a clear synergetic effect that the combined product is also a reliable reference for the tropospheric partial column.

We generate the combined $CH_4$ product for the time period between November 2017 and December 2019 and compare the individual and combined products to reference data of TCCON, AirCore and GAW. TCCON offers good references for $XCH_4$ and we get an agreement of all satellite $XCH_4$ products with the TCCON data within 1%. This comparison reveals a good reliability of the TROPOMI and the combined $XCH_4$ products, because of their independency on the a priori data (the comparison of the IASI data is affected by the a priori data and thus cannot be directly interpreted). We found that the AirCore data are a very good reference for the consistent validation of the $CH_4$ total column amounts and the $CH_4$ vertical distribution. Concerning total column comparison we get a very low $1\sigma$ scatter between the satellite products and the reference data (within 1%, which is similar to the comparison with TCCON). For the UTLS partial columns the scatter is also within 1% and for the tropospheric partial columns it is only slightly larger than 1%. While the comparison to TCCON shows no significant bias, here we find a positive bias in the combined total column averaged mixing ratios with respect to the AirCore references (significant

in the sense that the systematic difference is outside the $1\sigma$ scatter and that it can also be not explained by the uncertainty of the AirCore references). A significant bias is also found for the tropospheric partial column averaged mixing ratios. However, all these biases are rather low. For the combined product it is +1.1%±0.7% for the total column and +1.7%±1.2% for the tropospheric partial column.

We have only 24 AirCore profiles measured in collocation to satellite observations. A statistically more robust validation of the tropospheric partial column products can be achieved by using continuous $CH_4$ observations from two nearby GAW stations. The $CH_4$ signals that are common at both stations are a good validation reference for the troposphere. We get collocations between the GAW data and satellite observations for 95 individual days and the comparison to the tropospheric partial column averaged mixing ratios generated from the combined data product confirms and widens the conclusions based on the comparison with the AirCore data: for the comparison of the daily mean data we get a mean difference and $1\sigma$ scatter of +1.7%±1.2%, which is exactly the same as for the comparison with the AirCore data (i.e. the combined product agrees very well with reference data, but we find indications of a weak positive bias). The continuous GAW $CH_4$ reference data cover seasonal cycle signals and have a larger amplitude than the AirCore data. We demonstrate that the lower tropospheric partial column averaged mixing ratio generated from the combined data product is able to capture these signals much better than the respective IASI product or the TROPOMI total column averaged product.

The proposed method takes benefit from the outputs generated by the dedicated individual TROPOMI and IASI retrievals, it needs no extra retrievals, and is thus computationally very efficient. This makes it ideal for an application at large scale, and allows the combination of operational IASI and TROPOMI products in an efficient and sustained manner. This has a particular attraction, because IASI and TROPOMI successor instruments will be jointly aboard the upcoming Metop (Meteorological operational) Second Generation satellites (guaranteeing observations from the 2020s to the 2040s). There will be several 100,000 globally distributed and perfectly collocated observations (over land) of IASI and TROPOMI successor instruments per day, for which a combined product can be generated in a computationally very efficient way.

*Data availability.* Access to the MUSICA IASI data will soon be provided via http://www.imk-asf.kit.edu/english/musica-data.php (data access will become available during the second half of February 2021, for an earlier data provision please contact Matthias Schneider). The TROPOMI $XCH_4$ data used in this study are available for download at ftp://ftp.sron.nl/open-access-data-2/TROPOMI/tropomi/ch4/14_14_Lorente_et_al_2020_AMTD/. TCCON data are made available via the TCCON Data Archive, hosted by CaltechDATA, California Institute of Technology, California (USA), http://tccondata.org. For Trainou AirCore data please contact Michel Ramonet (michel.ramonet@lsce.ipsl.fr) and for Sodankylä AirCore data please contact Huilin Chen (huilin.chen@rug.nl). The GAW surface in-situ data are available via the World Data Centre for Greenhouse Gases (WDCGG), https://gaw.kishou.go.jp/search/.

## Appendix A: Theoretical considerations

In this appendix we give a brief overview on the theory of optimal estimation remote sensing methods. The focus is on the equations that are important for our work, i.e. the optimal a posteriori combination of two independently retrieved optimal

estimation remote sensing products. We show analytically that our method of combining two individually retrieved optimal estimation products by means of a posteriori calculations, is equivalent to a combined optimal estimation retrieval that uses a combined measurement vector.

For a more detailed and general insight into the theory of optimal estimation remote sensing methods we refer to Rodgers (2000) and for a general introduction on vector and matrix algebra dedicated textbooks are recommended.

## A1 Basics on retrieval theory

23-1

If we assume a moderately non-linear problem (according to Chapter 5 of Rodgers, 2000), the retrieved optimal estimation product (the retrieved atmospheric state vector $\hat{\boldsymbol{x}}$) can be written as:

$$\hat{\boldsymbol{x}} = \boldsymbol{x_a} + \mathbf{G}[\mathbf{K}(\boldsymbol{x} - \boldsymbol{x_a})]. \tag{A1}$$

Here $\boldsymbol{x}$ and $\boldsymbol{x_a}$ are the actual atmospheric state vector and the a priori atmospheric state vector, respectively. $\mathbf{K}$ is the Jacobian matrix, i,e, derivatives that capture how the measurement vector (the measured radiances) will change for changes of the atmospheric state (the atmospheric state vector $\boldsymbol{x}$). $\mathbf{G}$ is the gain matrix, i.e. derivatives that capture how the retrieved state vector will change for changes in the measurement vector:

$$\mathbf{G} = (\mathbf{K}^T {\mathbf{S_{y,n}}}^{-1} \mathbf{K} + {\mathbf{S_a}}^{-1})^{-1} \mathbf{K}^T {\mathbf{S_{y,n}}}^{-1}, \tag{A2}$$

with $\mathbf{S_{y,n}}$ and ${\mathbf{S_a}}^{-1}$ being the retrieval's noise covariance and the constraint matrices, respectively. In a strict optimal estimation sense, the constraint matrix is the inverse of the a priori covariance matrix $\mathbf{S_a}$.

The averaging kernel

$$\mathbf{A} = \mathbf{GK}, \tag{A3}$$

is an important component of a remote sensing retrieval, because according to Eq. (A1) it reveals how changes of the real atmospheric state vector $\boldsymbol{x}$ affect the retrieved atmospheric state vector $\hat{\boldsymbol{x}}$.

Very useful is also the a posteriori covariance matrix, which can be calculated as follows:

$$\mathbf{S}_{\hat{\boldsymbol{x}}} = (\mathbf{K}^T {\mathbf{S_{y,n}}}^{-1} \mathbf{K} + {\mathbf{S_a}}^{-1})^{-1}. \tag{A4}$$

The linearised formulation of the retrieval solution according to (A1) is very useful for the analytic characterisation of the product. The retrieval state's noise error covariance matrix for noise can be analytically calculated as:

$$\mathbf{S}_{\hat{\mathbf{x}},\mathbf{n}} = \mathbf{G}\mathbf{S}_{\mathbf{y},\mathbf{n}}\mathbf{G}^T, \tag{A5}$$

where $\mathbf{S_{y,n}}$ is the covariance matrix for noise on the measured radiances $\boldsymbol{y}$.

Further very helpful equations are the relations between the a posteriori covariance, the averaging kernel, the constraint (or the a priori covariance), and the retrieval's state noise error covariance matrices:

$$\mathbf{S}_{\hat{\boldsymbol{x}}} = (\mathbf{I} - \mathbf{A})\mathbf{S_a}, \tag{A6}$$

and

$$\mathbf{S}_{\hat{\boldsymbol{x}},\mathbf{n}} = \mathbf{A}\mathbf{S}_{\hat{\boldsymbol{x}}}, \tag{A7}$$

with $\mathbf{I}$ being the identity matrix.

### A2 Optimal combination of retrieval data products

In this subsection we discuss an optimal estimation retrieval that uses a combined measurement vector (two measurements from different instruments). Then we briefly introduce the Kalman filter and show that the Kalman filter formalism enables us to combine two individually retrieved remote sensing data products in equivalence to the optimal estimation retrieval using the combined measurement vector.

#### A2.1 Optimal estimation using a combined measurement vector

24-1

According to Eqs. (A1), (A2), and (A4) the retrieval product obtained from a combined measurement vector $\{\boldsymbol{y_1}, \boldsymbol{y_2}\}$ can be written as:

$$\begin{aligned}\hat{\boldsymbol{x}} - \boldsymbol{x_a} &= (\mathbf{K_1}^T \mathbf{S_{y_1,n}}^{-1} \mathbf{K_1} + \mathbf{K_2}^T \mathbf{S_{y_2,n}}^{-1} \mathbf{K_2} + \mathbf{S_a}^{-1})^{-1} (\mathbf{K_1}^T \mathbf{S_{y_1,n}}^{-1} \mathbf{K_1} + \mathbf{K_2}^T \mathbf{S_{y_2,n}}^{-1} \mathbf{K_2})(\boldsymbol{x} - \boldsymbol{x_a}) \\ &= (\mathbf{S}_{\hat{\boldsymbol{x}}_1}{}^{-1} + \mathbf{S}_{\hat{\boldsymbol{x}}_2}{}^{-1} - \mathbf{S_a}^{-1})^{-1} (\mathbf{K_1}^T \mathbf{S_{y_1,n}}^{-1} \mathbf{K_1} + \mathbf{K_2}^T \mathbf{S_{y_2,n}}^{-1} \mathbf{K_2})(\boldsymbol{x} - \boldsymbol{x_a}),\end{aligned} \tag{A8}$$

where $\mathbf{S_{y_1,n}}$ and $\mathbf{S_{y_2,n}}$ are the respective measurement noise covariances, $\mathbf{K_1}$ and $\mathbf{K_2}$ the respective Jacobians and $\mathbf{S}_{\hat{\boldsymbol{x}}_1}$ and $\mathbf{S}_{\hat{\boldsymbol{x}}_2}$ the respective a posteriori covariances.

#### A2.2 Linear Kalman filter

An important application of a Kalman filter (Kalman, 1960; Rodgers, 2000) is data assimilation in the context of atmospheric modelling. There the filter operates sequentially in different time steps. Kalman filter data assimilation methods determine the analysis state ($\hat{\boldsymbol{x}}^{\boldsymbol{a}}$) by optimally combining the background (or forecast) state ($\hat{\boldsymbol{x}}^{\boldsymbol{b}}$) with the information as provided by a new observation ($\hat{\boldsymbol{x}}^{\boldsymbol{o}}$):

$$\hat{\boldsymbol{x}}^{\boldsymbol{a}} = \hat{\boldsymbol{x}}^{\boldsymbol{b}} + \mathbf{M}[\hat{\boldsymbol{x}}^{\boldsymbol{o}} - \mathbf{H}\hat{\boldsymbol{x}}^{\boldsymbol{b}}]. \tag{A9}$$

Optimal means here that the uncertainties of both, the background state and the observation, are correctly taken into account by the Kalman gain matrix ($\mathbf{M}$):

$$\begin{aligned}\mathbf{M} &= \mathbf{S}_{\hat{\boldsymbol{x}}^b} \mathbf{H}^T (\mathbf{H}\mathbf{S}_{\hat{\boldsymbol{x}}^b}\mathbf{H}^T + \mathbf{S}_{\hat{\boldsymbol{x}}^o,\mathbf{n}})^{-1} \\ &= (\mathbf{H} + \mathbf{S}_{\hat{\boldsymbol{x}}^o_n} \mathbf{H}^{-T} \mathbf{S}_{\hat{\boldsymbol{x}}^b}{}^{-1})^{-1},\end{aligned} \tag{A10}$$

with $\mathbf{S}_{\hat{\boldsymbol{x}}^b}$ and $\mathbf{S}_{\hat{\boldsymbol{x}}^o,\mathbf{n}}$ being the uncertainty covariances of background state and the new measurement, respectively. The matrix $\mathbf{H}$ is the measurement forward operator, which maps the background domain into the measurement domain.

The similarity between Eqs. (A9) and (A10), on the one hand, and Eqs. (A1) and (A2), on the other hand, reveals that remote sensing optimal estimation and Kalman filter data assimilation methods use the same mathematical formalism.

### A2.3 Optimal a posteriori combination of individually retrieved data products

We have a first estimation of the atmospheric state (the first retrieval product $\hat{\boldsymbol{x}}_1$) and we want to optimally improve this estimation by using a second retrieval product ($\hat{\boldsymbol{x}}_2$). This is a typical data assimilation problem and we can use the Kalman filter formalism. We make the following settings:

$$\begin{aligned}\mathbf{S}_{\hat{\boldsymbol{x}}^b} &= \mathbf{S}_{\hat{\boldsymbol{x}}_1} \\ &= (\mathbf{K_1}^T \mathbf{S_{y_1,n}}^{-1} \mathbf{K_1} + \mathbf{S_a}^{-1})^{-1} \end{aligned} \tag{A11}$$

$$\begin{aligned}\mathbf{S}_{\hat{\boldsymbol{x}}^o,\mathbf{n}} &= \mathbf{S}_{\hat{\boldsymbol{x}}_2,\mathbf{n}} \\ &= (\mathbf{K_2}^T \mathbf{S_{y_2,n}}^{-1} \mathbf{K_2} + \mathbf{S_a}^{-1})^{-1} \mathbf{K_2}^T \mathbf{S_{y_2,n}}^{-1} \mathbf{K_2} (\mathbf{K_2}^T \mathbf{S_{y_2,n}}^{-1} \mathbf{K_2} + \mathbf{S_a}^{-1})^{-1} \\ &= \mathbf{S}_{\hat{\boldsymbol{x}}_2} \mathbf{K_2}^T \mathbf{S_{y_2,n}}^{-1} \mathbf{K_2} \mathbf{S}_{\hat{\boldsymbol{x}}_2} \end{aligned} \tag{A12}$$

$$\begin{aligned}\mathbf{H} &= \mathbf{A_2} \\ &= (\mathbf{K_2}^T \mathbf{S_{y_2,n}}^{-1} \mathbf{K_2} + \mathbf{S_a}^{-1})^{-1} \mathbf{K_2}^T \mathbf{S_{y_2,n}}^{-1} \mathbf{K_2} \\ &= \mathbf{S}_{\hat{\boldsymbol{x}}_2} \mathbf{K_2}^T \mathbf{S_{y_2,n}}^{-1} \mathbf{K_2} \end{aligned} \tag{A13}$$

$$\begin{aligned}\hat{\boldsymbol{x}}^b &= \hat{\boldsymbol{x}}_1 - \boldsymbol{x_a} \\ &= (\mathbf{K_1}^T \mathbf{S_{y_1,n}}^{-1} \mathbf{K_1} + \mathbf{S_a}^{-1})^{-1} \mathbf{K_1}^T \mathbf{S_{y_1,n}}^{-1} \mathbf{K_1} (\boldsymbol{x} - \boldsymbol{x_a}) \\ &= \mathbf{S}_{\hat{\boldsymbol{x}}_1} \mathbf{K_1}^T \mathbf{S_{y_1,n}}^{-1} \mathbf{K_1} (\boldsymbol{x} - \boldsymbol{x_a}) \end{aligned} \tag{A14}$$

$$\begin{aligned}\hat{\boldsymbol{x}}^o &= \hat{\boldsymbol{x}}_2 - \boldsymbol{x_a} \\ &= (\mathbf{K_2}^T \mathbf{S_{y_2,n}}^{-1} \mathbf{K_2} + \mathbf{S_a}^{-1})^{-1} \mathbf{K_2}^T \mathbf{S_{y_2,n}}^{-1} \mathbf{K_2} (\boldsymbol{x} - \boldsymbol{x_a}) \\ &= \mathbf{S}_{\hat{\boldsymbol{x}}_2} \mathbf{K_2}^T \mathbf{S_{y_2,n}}^{-1} \mathbf{K_2} (\boldsymbol{x} - \boldsymbol{x_a}). \end{aligned} \tag{A15}$$

In Eqs. (A11) and (A12) we assume that the two individual retrievals use the same constraint ($\mathbf{S_a}^{-1}$). This is generally not the case and we can a posteriori modify a constraint and its effect on state vectors and covariances by the formalism as presented in Chapter 10.4 of Rodgers (2000) or Sect. 4.2 of Rodgers and Connor (2003). For our problem here this is of secondary importance, because we assume that TROPOMI total column data products are almost independent on the constraint (as long as the constraint is reasonable).

In Eqs. (A14) and (A15) we assume the usage of the same a priori for the two individual retrievals. Since generally two indivudually performed retrievals use two different a priori settings we have to perform an a priori adjustment. Using the a priori of retrieval 2 as the reference ($\boldsymbol{x_{2,a}} = \boldsymbol{x_a}$) we can adjust the output of retrieval 1 by (see Eq. (10) of Rodgers and Connor, 2003):

$$\hat{\boldsymbol{x}}_1{}' = \hat{\boldsymbol{x}}_1 + (\mathbf{A_1} - \mathbf{I})(\boldsymbol{x_{1,a}} - \boldsymbol{x_{2,a}}), \tag{A16}$$

where $\boldsymbol{x_{1,a}}$ is the a priori used by retrieval 1.

Substitution of the settings from Eqs. (A11) - (A13) in Eq. (A10) gives:

$$\mathbf{M} = (\mathbf{S_{\hat{x}_1}}^{-1} + \mathbf{S_{\hat{x}_2}}^{-1} - \mathbf{S_a}^{-1})^{-1}\mathbf{S_{\hat{x}_2}}^{-1}, \tag{A17}$$

where we use Eqs. (A6) and (A7).

Substituting Eq. (A17) together with the settings from Eqs. (A14) and (A15) in Eq. (A9) finally yields:

$$\hat{\boldsymbol{x}}^{\boldsymbol{a}} - \boldsymbol{x_a} = (\mathbf{S_{\hat{x}_1}}^{-1} + \mathbf{S_{\hat{x}_2}}^{-1} - \mathbf{S_a}^{-1})^{-1}(\mathbf{K_1}^T\mathbf{S_{y_1,n}}^{-1}\mathbf{K_1} + \mathbf{K_2}^T\mathbf{S_{y_2,n}}^{-1}\mathbf{K_2})(\boldsymbol{x} - \boldsymbol{x_a}), \tag{A18}$$

i.e. the analysis state is the same as the output $\hat{\boldsymbol{x}}$ of a retrieval with a combined measurement vector from Eq. (A8). This means that we can a posteriori calculate the result that would be obtained by an optimal estimation retrieval using a combined measurement vector.

### A2.4 Requirements

The optimal a posteriori combination of two remote sensing products is possible, whenever: (1) the two remote sensing observations are made at the same time and detect the same location, (2) the problem is moderately non-linear (according to Chapter 5 of Rodgers, 2000), and (3) the individual retrieval output as listed by Eqs. (A11) to (A15) is made available. This is for the first retrieval the aposteriori covariances ($\mathbf{S_{\hat{x}}}$, which might also be reconstracted from $\mathbf{A}$ and $\mathbf{R}$ according to Eq. (A6)), the averaging kernels ($\mathbf{A}$), and the retrieved and a priori state vectors ($\hat{\boldsymbol{x}}$ and $\boldsymbol{x_a}$, respectively). For the second retrieval we need the noise covariances ($\mathbf{S_{\hat{x},n}}$), the averaging kernels ($\mathbf{A}$), and the retrieved and a priori state vectors ($\hat{\boldsymbol{x}}$ and $\boldsymbol{x_a}$, respectively).

## Appendix B: Operator for transformation between linear and logarithmic scales

Linear scale differentials and logarithmic scale differentials are related by $\Delta x = x\Delta \ln x$. For transforming differentials or covariances of a state vector with dimension $nal$ ($nal$: number of atmospheric levels) from logarithmic to linear scale we define the $nal \times nal$ diagonal matrix $\mathbf{L}$:

$$\mathbf{L} = \begin{pmatrix} \hat{x}_1 & 0 & \cdots & 0 \\ 0 & \hat{x}_2 & \cdots & 0 \\ \vdots & \vdots & \ddots & \vdots \\ 0 & 0 & \cdots & \hat{x}_{nal} \end{pmatrix}. \tag{B1}$$

Here $\hat{x}_i$ is the value of the $i$th element of the retrieved state vector (i.e. in case of an atmospheric $CH_4$ state vector the $CH_4$ mixing ratios retrieved at the $i$th model level).

A logarithmic scale averaging kernel matrix $\mathbf{A^l}$ can then be expressed in the linear scale as:

$$\mathbf{A} = \mathbf{L}\mathbf{A^l}\mathbf{L}^{-1}. \tag{B2}$$

Similarly a logarithmnic scale covariance matrix $\mathbf{S^l}$ can then be expressed in the linear scale as:

$$\mathbf{S} = \mathbf{L}\mathbf{S^l}\mathbf{L}^T. \tag{B3}$$

## Appendix C: Operators for column data

This appendix explains the calculation of operators for partial (and total) column data. Although some sections are similar to Appendix C of Schneider et al. (2021) we think it is here a very useful reference, because it facilitates the reproducibility of our results.

For converting mixing ratio profiles into amount profiles we set up a pressure weighting operator $\mathbf{Z}$, as a diagonal matrix with the following entries:

$$Z_{i,i} = \frac{\Delta p_i}{g_i m_{\mathrm{air}} (1 + \frac{m_{\mathrm{H_2O}}}{m_{\mathrm{air}}} \hat{x}_i^{\mathrm{H_2O}})}. \tag{C1}$$

Using the pressure $p_i$ at atmospheric grid level $i$ we set $\Delta p_1 = \frac{p_2 - p_1}{2} - p_1$, $\Delta p_{nal} = p_{nal} - \frac{p_n al - p_{nal-1}}{2}$, and $\Delta p_i = \frac{p_{i+1} - p_i}{2} - \frac{p_i - p_{i-1}}{2}$ for $1 < i < nal$. Furthermore, $g_i$ is the gravitational acceleration at level $i$, $m_{\mathrm{air}}$ and $m_{\mathrm{H_2O}}$ the molecular mass of dry air and water vapour, respectively, and $\hat{x}_i^{\mathrm{H_2O}}$ the retrieved or modelled water vapour mixing ratio at level $i$.

We define an operator $\mathbf{W}$ for resampling fine gridded atmospheric amount profiles into coarse gridded atmospheric partial column amount profiles. It has the dimension $c \times nal$, where $c$ is the number of the resampled coarse atmospheric grid levels and $nal$, the number of atmospheric levels of the original fine atmospheric grid. Each line of the operator has the value '1' for the levels that are resampled and '0' for all other levels:

$$\mathbf{W} = \begin{pmatrix} 1 & \cdots & 1 & 0 & \cdots & \cdots & \cdots & \cdots & 0 \\ 0 & \cdots & 0 & 1 & \cdots & 1 & 0 & \cdots & 0 \\ 0 & \cdots & \cdots & \cdots & \cdots & 0 & 1 & \cdots & 1 \end{pmatrix}. \tag{C2}$$

In analogy we can define a row vector $\boldsymbol{w}^T$ (with the dimension $1 \times nal$) with all elements having the value '1', which allows the resampling for the total column amounts.

### C1 Column amounts

The kernel that discribes how a change in the amount at a certain altitude affects the retrieved partial (or total) colunm amount can be calculated as:

$$\mathbf{A}' = \mathbf{WZAZ}^{-1}. \tag{C3}$$

For the total column we replace $\mathbf{W}$ by $\boldsymbol{w}^T$ and get the row vector $\boldsymbol{a'}^T$ (dimension $1 \times nal$). This is the total column kernel provided by the TROPOMI data and it is typically written as $\boldsymbol{a}^T$. Figure 3 shows examples of such total and partial columns amount kernels. The total column amount kernel can be interpolated to different altitude grids. For the applications in Sects. 2 and 3 we interpolate the TROPOMI total column amount kernel to the vertical grid used by the MUSICA IASI retrieval.

### C2 Column averaged mixing ratios

We can also combine the operators $\mathbf{Z}$ and $\mathbf{W}$ for the calculation of a pressure weighted resampling operator by:

$$\mathbf{W}^* = (\mathbf{WZW}^T)^{-1}\mathbf{WZ}. \tag{C4}$$

This operator resamples linear scale mixing ratio profiles into linear scale partial column averaged mixing ratio profiles. Its inverse is calculated as:

$$\mathbf{W}^{*-1} = \mathbf{Z}^{-1}\mathbf{W}^{-1}(\mathbf{W}\mathbf{Z}\mathbf{W}^{T}), \tag{C5}$$

with $\mathbf{W}^{-1} = (\mathbf{W}^{T}\mathbf{W})^{-1}\mathbf{W}^{T}$. The respective total column operators $\boldsymbol{w}^{*T}$ and $(\boldsymbol{w}^{*T})^{-1}$ can be calculated in analogy by replacing $\mathbf{W}$ by $\boldsymbol{w}^{T}$.

With operator $\mathbf{W}^{*}$ we can calculate a coarse gridded partial column averaged state $\hat{\boldsymbol{x}}^{*}$ from the fine gridded linear mixing ratio state $\hat{\boldsymbol{x}}$ by:

$$\hat{\boldsymbol{x}}^{*} = \mathbf{W}^{*}\hat{\boldsymbol{x}}. \tag{C6}$$

The kernels matrix of the partial column averaged mixing ratio state can then be calculated from the fine gridded linear scale kernel matrix ($\mathbf{A}$) by:

$$\mathbf{A}^{*} = \mathbf{W}^{*}\mathbf{A}. \tag{C7}$$

28-1

This kernel discribes how a change in the mixing ratio at a certain altitude affects the retrieved partial ~~column~~ averaged mixing ratio. Covariances of the partial column averaged mixing ratio state can be calculated from the corresponding covariance matrices of the fine gridded linear scale ($\mathbf{S}$) by:

$$\mathbf{S}^{*} = \mathbf{W}^{*}\mathbf{S}\mathbf{W}^{*T}. \tag{C8}$$

The respective calculations for total column averaged mixing ratios can be made by replacing $\mathbf{W}^{*}$ by $\boldsymbol{w}^{*T}$. For the total column avereraged mixing ratios the covariance is a simple variance (the scalar $\mathbf{S}^{*}$) and the kernel has the dimension $1 \times nol$, i.e. it is a row vector $\boldsymbol{a}^{*T}$.

The total column amount kernel ($\boldsymbol{a_T}^{T}$) provided with the TROPOMI data set can be converted into a total column averaged mixing ratio kernel $\boldsymbol{a}^{*}_{\boldsymbol{T}}{}^{T}$ by the following calculation:

$$\boldsymbol{a}^{*}_{\boldsymbol{T}}{}^{T} = \boldsymbol{w}^{*T}\mathbf{A} = (\boldsymbol{w}^{T}\mathbf{Z}\boldsymbol{w})^{-1}\boldsymbol{a_T}^{T}\mathbf{Z}. \tag{C9}$$

The total column averaged mixing ratio kernel $\boldsymbol{a}^{*}_{\boldsymbol{T}}{}^{T}$ used in Sects. 2 and 3 is valid for the vertical grid used by the MUSICA IASI retrieval. It is calculated according to Eq. (C9), but using a TROPOMI total column amount kernel ($\boldsymbol{a_T}$) that is interpolated onto the MUSICA IASI grid (see also Appendix C1).

*Author contributions.* Matthias Schneider developed the idea for the optimal a posteriori combination of two remote sensing products and he prepared the figures and the manuscript. Benjamin Ertl developed and performed the continuous MUSICA IASI data processing, where he was supported by Matthias Schneider, Christopher J. Diekmann, Farahnaz Khosrawi, Amelie N. Röhling, Omaira E. García, and Eliezer Sepúlveda. Frank Hase developed the PROFFIT-nadir retrieval code used for the MUSICA IASI processing. Tobias Borsdorff, Jochen Landgraf, and Alba Lorente are responsible for the TROPOMI processing and made TROPOMI data available. Huilin Chen

and Rigel Kivi provided the AirCore profile measurements over Sodankylä and Thomas Laemmel and Michel Ramonet provided the AirCore profile measurements over Trainou. Martin Steinbacher and Frank Meinhardt are responsible for the GAW data of Jungfraujoch and Schauinsland, respectively. Rigel Kivi, Darko Dubravica, Frank Hase, Voltaire A. Velazco, David W. T. Griffith, Nicholas M. Deutscher, and David F. Pollard are responsible for the TCCON data from Sodankylä, Karlsruhe, Burgos, Darwin, Wollongong, and Lauder. All authors supported the generation of the final version of this manuscript.

*Competing interests.* The authors declare that they have no conflict of interest

*Acknowledgements.* This research has largely benefit from funds of the Deutsche Forschungsgemeinschaft (provided for the two projects MOTIV and TEDDY with IDs/Geschäftszeichen 290612604/GZ:SCHN1126/2-1 and 416767181/GZ:SCHN1126/5-1, respectively) and from support by the European Space Agency in the context the "Sentinel-5p+Innovation (S5p+I) - Water Vapour Isotopologues (H2O-ISO)" activities. Furthermore, we acknowledge funds from the Ministerio de Economía y Competividad from Spain for the project INMENSE (CGL2016-80688-P).

Important part of this work was performed on the supercomputer ForHLR funded by the Ministry of Science, Research and the Arts Baden-Württemberg and by the German Federal Ministry of Education and Research. We also acknowledge the contribution of Teide High-Performance Computing facilities. TeideHPC facilities are provided by the Instituto Tecnológico y de Energías Renovables (ITER), S.A (teidehpc.iter.es).

The TROPOMI data processing was carried out on the Dutch National e-Infrastructure with the support of the SURF cooperative. The presented material contains modified Copernicus data (2017, 2019).

The Karlsruhe TCCON station has been supported by the German Bundesministerium für Wirtschaft und Energie (BMWi) via DLR under grants 50EE1711A to E and by the Helmholtz Society via the research program ATMO. The Burgos TCCON site is supported in part by the GOSAT series project. Burgos is supported in part by the Energy Development Corp. Philippines. The Lauder TCCON programme is core funded by NIWA through New Zealand's Ministry of Business, Innovation and Employment. NMD is funded by ARC Future Fellowship FT180100327. Darwin and Wollongong TCCON stations are supported by ARC grants DP160100598, LE0668470, DP140101552, DP110103118 and DP0879468, and Darwin through NASA grants NAG5-12247 and NNG05-GD07G.

The Trainou AirCore measurements have been supported by CEA, CNES, UVSQ, IPSL and the EU H2020 RINGO project (GA no. 730944), and are part of the French consortium for Aircore measurements (LMD, LSCE, GSMA, CNES). The Sodankylä TCCON and AirCore measurements have been supported via the ESA FRM4GHG project (under the grant agreement no. ESA-IPLPOE-LG-cl-LE-2015-1129) and the EU H2020 RINGO project.

The $CH_4$ observations at Jungfraujoch were established as part of the Swiss National Air Pollution Monitoring Network and are supported through ICOS-CH, which is funded by the Swiss National Science Foundation and in-house contributions.

We acknowledge the support by the Deutsche Forschungsgemeinschaft and the Open Access Publishing Fund of the Karlsruhe Institute of Technology.

## References


Borger, C., Schneider, M., Ertl, B., Hase, F., García, O. E., Sommer, M., Höpfner, M., Tjemkes, S. A., and Calbet, X.: Evaluation of MUSICA IASI tropospheric water vapour profiles using theoretical error assessments and comparisons to GRUAN Vaisala RS92 measurements, Atmospheric Measurement Techniques, 11, 4981–5006, https://doi.org/10.5194/amt-11-4981-2018, https://www.atmos-meas-tech.net/11/4981/2018/, 2018.

Butz, A., Guerlet, S., Hasekamp, O., Schepers, D., Galli, A., Aben, I., Frankenberg, C., Hartmann, J.-M., Tran, H., Kuze, A., Keppel-Aleks, G., Toon, G., Wunch, D., Wennberg, P., Deutscher, N., Griffith, D., Macatangay, R., Messerschmidt, J., Notholt, J., and Warneke, T.: Toward accurate CO2 and CH4 observations from GOSAT, Geophysical Research Letters, 38, https://doi.org/https://doi.org/10.1029/2011GL047888, https://agupubs.onlinelibrary.wiley.com/doi/abs/10.1029/2011GL047888, 2011.

Ceccherini, S., Raspollini, P., and Carli, B.: Optimal use of the information provided by indirect measurements of atmospheric vertical profiles, Opt. Express, 17, 4944–4958, https://doi.org/10.1364/OE.17.004944, http://www.opticsexpress.org/abstract.cfm?URI=oe-17-7-4944, 2009.

Cortesi, U., Del Bianco, S., Ceccherini, S., Gai, M., Dinelli, B. M., Castelli, E., Oelhaf, H., Woiwode, W., Höpfner, M., and Gerber, D.: Synergy between middle infrared and millimeter-wave limb sounding of atmospheric temperature and minor constituents, Atmospheric Measurement Techniques, 9, 2267–2289, https://doi.org/10.5194/amt-9-2267-2016, https://amt.copernicus.org/articles/9/2267/2016/, 2016.

Costantino, L., Cuesta, J., Emili, E., Coman, A., Foret, G., Dufour, G., Eremenko, M., Chailleux, Y., Beekmann, M., and Flaud, J.-M.: Potential of multispectral synergism for observing ozone pollution by combining IASI-NG and UVNS measurements from the EPS-SG satellite, Atmospheric Measurement Techniques, 10, 1281–1298, https://doi.org/10.5194/amt-10-1281-2017, https://www.atmos-meas-tech.net/10/1281/2017/, 2017.

Cuesta, J., Eremenko, M., Liu, X., Dufour, G., Cai, Z., Höpfner, M., von Clarmann, T., Sellitto, P., Foret, G., Gaubert, B., Beekmann, M., Orphal, J., Chance, K., Spurr, R., and Flaud, J.-M.: Satellite observation of lowermost tropospheric ozone by multispectral synergism of IASI thermal infrared and GOME-2 ultraviolet measurements over Europe, Atmospheric Chemistry and Physics, 13, 9675–9693, https://doi.org/10.5194/acp-13-9675-2013, https://www.atmos-chem-phys.net/13/9675/2013/, 2013.

Diekmann, C. J., Schneider, M., Ertl, B., Hase, F., Khosrawi, F., García, O. E., Sepúlveda, E., Knippertz, P., and Braesicke, P.: The MUSICA IASI {$H_2O$,$\delta$D} pair product, currently in preparation for Earth System Science Data, 2021.

García, O. E., Schneider, M., Ertl, B., Sepúlveda, E., Borger, C., Diekmann, C., Wiegele, A., Hase, F., Barthlott, S., Blumenstock, T., Raffalski, U., Gómez-Peláez, A., Steinbacher, M., Ries, L., and de Frutos, A. M.: The MUSICA IASI $CH_4$ and $N_2O$ products and their comparison to HIPPO, GAW and NDACC FTIR references, Atmospheric Measurement Techniques, 11, 4171–4215, https://doi.org/10.5194/amt-11-4171-2018, https://www.atmos-meas-tech.net/11/4171/2018/, 2018.

Griffith, D. W., Deutscher, N. M., Velazco, V. A., Wennberg, P. O., Yavin, Y., Keppel-Aleks, G., Washenfelder, R. A., Toon, G. C., Blavier, J.-F., Paton-Walsh, C., Jones, N. B., Kettlewell, G. C., Connor, B. J., Macatangay, R. C., Roehl, C., Ryczek, M., Glowacki, J., Culgan, T., and Bryant, G. W.: TCCON data from Darwin (AU), Release GGG2014.R0, https://doi.org/10.14291/TCCON.GGG2014.DARWIN01.R0/1149290, https://data.caltech.edu/records/269, 2014a.

Griffith, D. W., Velazco, V. A., Deutscher, N. M., Paton-Walsh, C., Jones, N. B., Wilson, S. R., Macatangay, R. C., Kettlewell, G. C., Buchholz, R. R., and Riggenbach, M. O.: TCCON data from Wollongong (AU), Release GGG2014.R0, https://doi.org/10.14291/TCCON.GGG2014.WOLLONGONG01.R0/1149291, https://data.caltech.edu/records/291, 2014b.

Hase, F., Blumenstock, T., Dohe, S., Groß, J., and Kiel, M.: TCCON data from Karlsruhe (DE), Release GGG2014.R1, https://doi.org/10.14291/TCCON.GGG2014.KARLSRUHE01.R1/1182416, https://data.caltech.edu/records/278, 2015.

Hasekamp, O., Lorente, A., Hu, H., Butz, A., aan de Brugh, J., and Landgraf, J.: Algorithm Theoretical Baseline Document for Senitinel-5 Precursor methane retrieval, http://www.tropomi.eu/documents/atbd/, 2019.

Hu, H., Hasekamp, O., Butz, A., Galli, A., Landgraf, J., Aan de Brugh, J., Borsdorff, T., Scheepmaker, R., and Aben, I.: The operational methane retrieval algorithm for TROPOMI, Atmospheric Measurement Techniques, 9, 5423–5440, https://doi.org/10.5194/amt-9-5423-2016, https://amt.copernicus.org/articles/9/5423/2016/, 2016.

Kalman, R. E.: A new approach to linear filtering and prediction problems, J. Basic Eng., 82, 35, 1960.

Karion, A., Sweeney, C., Tans, P., and Newberger, T.: AirCore: An Innovative Atmospheric Sampling System, Journal of Atmospheric and Oceanic Technology, 27, 1839 – 1853, https://doi.org/10.1175/2010JTECHA1448.1, https://journals.ametsoc.org/view/journals/atot/27/11/2010jtecha1448_1.xml, 2010.

Keppens, A., Lambert, J.-C., Granville, J., Miles, G., Siddans, R., van Peet, J. C. A., van der A, R. J., Hubert, D., Verhoelst, T., Delcloo, A., Godin-Beekmann, S., Kivi, R., Stübi, R., and Zehner, C.: Round-robin evaluation of nadir ozone profile retrievals: methodology and application to MetOp-A GOME-2, Atmospheric Measurement Techniques, 8, 2093–2120, https://doi.org/10.5194/amt-8-2093-2015, https://www.atmos-meas-tech.net/8/2093/2015/, 2015.

Kivi, R. and Heikkinen, P.: Fourier transform spectrometer measurements of column $CO_2$ at Sodankylä, Finland, Geoscientific Instrumentation, Methods and Data Systems, 5, 271–279, https://doi.org/10.5194/gi-5-271-2016, https://gi.copernicus.org/articles/5/271/2016/, 2016.

Kivi, R., Heikkinen, P., and Kyrö, E.: TCCON data from Sodankylä (FI), Release GGG2014.R0, https://doi.org/10.14291/TCCON.GGG2014.SODANKYLA01.R0/1149280, https://data.caltech.edu/records/289, 2014.

Krol, M., Houweling, S., Bregman, B., van den Broek, M., Segers, A., van Velthoven, P., Peters, W., Dentener, F., and Bergamaschi, P.: The two-way nested global chemistry-transport zoom model TM5: algorithm and applications, Atmospheric Chemistry and Physics, 5, 417–432, https://doi.org/10.5194/acp-5-417-2005, https://acp.copernicus.org/articles/5/417/2005/, 2005.

Landgraf, J., Butz, A., Hasekamp, O., Hu, H., , and aan de Brugh, J.: Senitinel 5 L2 Prototype Processors, Algorithm Theoretical Baseline Document: Methane Retrieval, 2019.

Lorente, A., Borsdorff, T., Butz, A., Hasekamp, O., aan de Brugh, J., Schneider, A., Hase, F., Kivi, R., Wunch, D., Pollard, D. F., Shiomi, K., Deutscher, N. M., Velazco, V. A., Roehl, C. M., Wennberg, P. O., Warneke, T., and Landgraf, J.: Methane retrieved from TROPOMI: improvement of the data product and validation of the first two years of measurements, Atmospheric Measurement Techniques Discussions, 2020, 1–28, https://doi.org/10.5194/amt-2020-281, https://amt.copernicus.org/preprints/amt-2020-281/, 2020.

Pandey, S., Houweling, S., Krol, M., Aben, I., Chevallier, F., Dlugokencky, E. J., Gatti, L. V., Gloor, E., Miller, J. B., Detmers, R., Machida, T., and Röckmann, T.: Inverse modeling of GOSAT-retrieved ratios of total column $CH_4$ and $CO_2$ for 2009 and 2010, Atmospheric Chemistry and Physics, 16, 5043–5062, https://doi.org/10.5194/acp-16-5043-2016, https://acp.copernicus.org/articles/16/5043/2016/, 2016.

Parker, R. J., Webb, A., Boesch, H., Somkuti, P., Barrio Guillo, R., Di Noia, A., Kalaitzi, N., Anand, J. S., Bergamaschi, P., Chevallier, F., Palmer, P. I., Feng, L., Deutscher, N. M., Feist, D. G., Griffith, D. W. T., Hase, F., Kivi, R., Morino, I., Notholt, J., Oh, Y.-S., Ohyama, H., Petri, C., Pollard, D. F., Roehl, C., Sha, M. K., Shiomi, K., Strong, K., Sussmann, R., Té, Y., Velazco, V. A., Warneke, T., Wennberg, P. O., and Wunch, D.: A decade of GOSAT Proxy satellite $CH_4$ observations, Earth System Science Data, 12, 3383–3412, https://doi.org/10.5194/essd-12-3383-2020, https://essd.copernicus.org/articles/12/3383/2020/, 2020.

Pollard, D. F., Robinson, J., and Shiona, H.: TCCON data from Lauder (NZ), Release GGG2014.R0, https://doi.org/10.14291/TCCON.GGG2014.LAUDER03.R0, https://data.caltech.edu/records/1220, 2019.

Rodgers, C.: Inverse Methods for Atmospheric Sounding: Theory and Praxis, World Scientific Publishing Co., Singapore, 2000.

Rodgers, C. and Connor, B.: Intercomparison of remote sounding instruments, J. Geophys. Res., 108, 4116–4129, https://doi.org/10.1029/2002JD002299, 2003.

Schneider, M., Wiegele, A., Barthlott, S., González, Y., Christner, E., Dyroff, C., García, O. E., Hase, F., Blumenstock, T., Sepúlveda, E., Mengistu Tsidu, G., Takele Kenea, S., Rodríguez, S., and Andrey, J.: Accomplishments of the MUSICA project to provide accurate, long-term, global and high-resolution observations of tropospheric {$H_2O$,$\delta$D} pairs – a review, Atmospheric Measurement Techniques, 9, 2845–2875, https://doi.org/10.5194/amt-9-2845-2016, http://www.atmos-meas-tech.net/9/2845/2016/, 2016.

Schneider, M., Ertl, B., Diekmann, C., Khosrawi, F., Weber, A., Hase, F., Höpfner, M. García, O. E., Sepúlveda, E., and Kinnison, D.: Design and description of the MUSICA IASI full retrieval product, submitted to Earth Systems Science Data, 2021.

Sepúlveda, E., Schneider, M., Hase, F., Barthlott, S., Dubravica, D., García, O. E., Gomez-Pelaez, A., González, Y., Guerra, J. C., Gisi, M., Kohlhepp, R., Dohe, S., Blumenstock, T., Strong, K., Weaver, D., Palm, M., Sadeghi, A., Deutscher, N. M., Warneke, T., Notholt, J., Jones, N., Griffith, D. W. T., Smale, D., Brailsford, G. W., Robinson, J., Meinhardt, F., Steinbacher, M., Aalto, T., and Worthy, D.: Tropospheric $CH_4$ signals as observed by NDACC FTIR at globally distributed sites and comparison to GAW surface in situ measurements, Atmospheric Measurement Techniques, 7, 2337–2360, https://doi.org/10.5194/amt-7-2337-2014, https://amt.copernicus.org/articles/7/2337/2014/, 2014.

Sherlock, V., Connor, B., Robinson, J., Shiona, H., Smale, D., and Pollard, D. F.: TCCON data from Lauder (NZ), 125HR, Release GGG2014.R0, https://doi.org/10.14291/TCCON.GGG2014.LAUDER02.R0/1149298, https://data.caltech.edu/records/281, 2014.

Velazco, V. A., Morino, I., Uchino, O., Hori, A., Kiel, M., Bukosa, B., Deutscher, N. M., Sakai, T., Nagai, T., Bagtasa, G., Izumi, T., Yoshida, Y., and Griffith, D. W. T.: TCCON Philippines: First Measurement Results, Satellite Data and Model Comparisons in Southeast Asia, Remote Sensing, 9, https://doi.org/10.3390/rs9121228, https://www.mdpi.com/2072-4292/9/12/1228, 2017.

Wagenhäuser, T., Engel, A., and Sitals, R.: Testing the altitude attribution and vertical resolution of AirCore measurements with a new spiking method, Atmospheric Measurement Techniques Discussions, 2021, 1–18, https://doi.org/10.5194/amt-2020-461, https://amt.copernicus.org/preprints/amt-2020-461/, 2021.

Worden, J. R., Turner, A. J., Bloom, A., Kulawik, S. S., Liu, J., Lee, M., Weidner, R., Bowman, K., Frankenberg, C., Parker, R., and Payne, V. H.: Quantifying lower tropospheric methane concentrations using GOSAT near-IR and TES thermal IR measurements, Atmospheric Measurement Techniques, 8, 3433–3445, https://doi.org/10.5194/amt-8-3433-2015, https://amt.copernicus.org/articles/8/3433/2015/, 2015.

Wunch, D., Toon, G. C., Blavier, J.-F. L., Washenfelder, R. A., Notholt, J., Connor, B. J., Griffith, D. W. T., Sherlock, V., and Wennberg, P. O.: The Total Carbon Column Observing Network, Philosophical Transactions of the Royal Society A: Mathematical, Physical and Engineering Sciences, 369, 2087–2112, https://doi.org/10.1098/rsta.2010.0240, https://royalsocietypublishing.org/doi/abs/10.1098/rsta.2010.0240, 2011.

2-1 May 11, 2021 at 9:11 PM, Reviewer
There are quite a few more examples in the literature than those mentioned. In particular they neglect Landgraf and Hasekamp (2007), Worden et al, (2007), Fu et al, (2013), (2018), etc. Authors need to do more diligence with their citations.

3-1 May 11, 2021 at 9:11 PM, Reviewer
This approach was discussed in detail in Lou et al, 2013 with TES and MLS data.

3-2 May 11, 2021 at 9:11 PM, Reviewer
The tropopause will be an issue for profile retrievals as well. This argument needs to be more quantitative about how uncertainties in tropopause height will affect the xCH4 calculation.

4-1 May 19, 2021 at 10:14 PM, Reviewer
Order

4-2 May 19, 2021 at 10:14 PM, Reviewer
I don't think it's appropriate to cite a paper in prep. It at least needs to be in review.

6-1 May 19, 2021 at 10:14 PM, Reviewer
These two instruments are in fundamentally different orbits and therefore different local solar times. The difference in LST is already about 4 hours. To the extent to which the variability in either is driven by dynamics, then this difference could be substantial. In particular, the PBL heights could be quite different. The criteria described here appear to be arbitrary. In additional analysis motivating these choices needs to be included (these figure could be added in an appendix).

The assumption that the vertical distribution between morning and afternoon is relatively unchanged is an important assumption. This could be further tested by looking at CAMS CH4 output and showing in an OSSE framework that the sampling assumption here hold.

8-1 May 19, 2021 at 10:14 PM, Reviewer
In Fig. 3, it looks like the a priori contribution for TROPOMI is negative. Can you explain why?

11-1 May 24, 2021 at 8:55 PM, Reviewer
These criteria appear to be driven primarily by pragmatic considerations rather minimization of error from two different locations. The authors need to demonstrate what the theoretical considerations for this to work.

12-1 May 24, 2021 at 8:55 PM, Reviewer
Under what basis is this assumption made? Why should this be considered to reasonably capture the error?

13-1 May 24, 2021 at 8:55 PM, Reviewer
Please include on the other axis the absolute differences ppb.

13-2 May 24, 2021 at 8:55 PM, Reviewer
IASI has a positive bias relative to TCCON but TROPOMI has a negative bias. The combined product is substantially closer to IASI than TROPOMI. Please explain.

13-3 May 24, 2021 at 8:55 PM, Reviewer
Add a figure comparing the agreement between the a priori and TCCON. Or at least, calculate it and provide the summary statistics for comparison with the retrievals .

13-4 May 24, 2021 at 8:55 PM, Reviewer
Please add the offset in addition to the slope.

14-1 May 24, 2021 at 8:55 PM, Reviewer
agreement

14-2 May 24, 2021 at 8:55 PM, Reviewer
How do you justify that R^2=0.5 is good agreement? The combined product is not appreciably better than the individual products. Is the reason for the low correlation the time-space difference error? Explain.

15-1 May 24, 2021 at 8:55 PM, Reviewer
An important difference is that in this case the bias is not positive relative to AirCore but negative relative to TCCON. Please explain.

15-2 May 24, 2021 at 8:55 PM, Reviewer
Not really clear. Please elaborate as to why the AirCore is substantially worse. One particular point is that TCCON is a remote sensing measurement whereas AirCore is not. The impact of vertical differences will be more pronounced.

18-1 May 24, 2021 at 8:55 PM, Reviewer
That would satisfy a “do no harm” case, but how does this show that the combined product is better than the individual product(s)?

21-1 May 24, 2021 at 8:55 PM, Reviewer
You can and should assess that by correlating GAW with the IASI prior.

21-2 May 24, 2021 at 8:55 PM, Reviewer
That’s not been demonstrated. In particular, the assumption is that the problem is linear, which the authors have not shown. Rather, we know that the problem is non-linear, which is not resolved by the derivation in the Appendix.

21-3 May 24, 2021 at 8:55 PM, Reviewer
It’s not real clear what is being gained here. The combined product suffers from errors due to dislocation that are not quantified. Why do I need a combined product if I already have each product individually, which have the sensitivities to the UTLS and total column?

21-4 May 24, 2021 at 8:55 PM, Reviewer
It would be good to capitulate those improvements here as they are still not clear.

23-1 May 24, 2021 at 8:55 PM, Reviewer
For this derivation, the definition of moderate non-linearity is quite important as well as its limitations. The assertions made earlier about equivalence with a radiance-based retrieval hinge on it. Please elaborate and discuss relationship with radiance-based retrievals.

24-1 May 24, 2021 at 8:55 PM, Reviewer
While this derivation is well-known, the important assumption is that the two measurement vectors are measuring the same atmosphere. However, for IASI and TROPOMI, that is not the case at all. So, y1=F(x1)+n1 and y2=F(x2)+n2. A more interesting and theoretically necessary question for this paper is the error introduced by x1 not-equal x2. At what point is that error negligible? What are the atmospheric conditions necessary for that to be the case? That could be readily studied by sampling a model such as CAMS and building linear retrievals of both for IASI and TROPOMI in their respective orbit.

28-1 May 24, 2021 at 8:55 PM, Reviewer
column